Biomedicine & Pharmacotherapy 165 (2023) 115023

Contents lists available at ScienceDirect

Biomedicine & Pharmacotherapy

journal homepage: www.elsevier.com/locate/biopha

Dual receptor specific nanoparticles targeting EGFR and PD-L1 for enhanced delivery of docetaxel in cancer therapy

Fakhrossadat Emami [a,1], Ramesh Duwa [a,1], Asmita Banstola [a,b], Seon Min Woo [c], Taeg Kyu Kwon [c], Simmyung Yook [a,*]

[a] College of Pharmacy, Keimyung University, 1095 Dalgubeol-daero, Dalseo-Gu, Daegu 42601, the Republic of Korea
[b] Wellman Center for Photomedicine, Massachusetts General Hospital, Department of Dermatology, Harvard Medical School, Boston, MA, 02114, USA
[c] Department of Immunology, School of Medicine, Keimyung University, Daegu 42601, the Republic of Korea

ARTICLE INFO

Keywords:
Poly(lactide-co-glycolide) acid
Docetaxel
Dual-ligand
Single-ligand
Nanoparticle
Affinity

ABSTRACT

Dual-receptor targeted (DRT) nanoparticles which contain two distinct targeting agents may exhibit higher cell selectivity, cellular uptake, and cytotoxicity toward cancer cells than single-ligand targeted nanoparticle systems without additional functionality. The purpose of this study is to prepare DRT poly(lactic-co-glycolic acid) (PLGA) nanoparticles for targeting the delivery of docetaxel (DTX) to the EGFR and PD-L1 receptor positive cancer cells such as human glioblastoma multiform (U87-MG) and human non-small cell lung cancer (A549) cell lines. Anti-EGFR and anti-PD-L1 antibody were decorated on DTX loaded PLGA nanoparticles to prepare DRT-DTX-PLGA via. single emulsion solvent evaporation method. Physicochemical characterizations of DRT-DTX-PLGA, such as particle size, zeta-potential, morphology, and *in vitro* DTX release were also evaluated. The average particle size of DRT-DTX-PLGA was 124.2 ± 1.1 nm with spherical and smooth morphology. In the cellular uptake study, the DRT-DTX-PLGA endocytosed by the U87-MG and A549 cells was single ligand targeting nanoparticle. From the *in vitro* cell cytotoxicity, and apoptosis studies, we reported that DRT-DTX-PLGA exhibited high cytotoxicity and enhanced the apoptotic cell compared to the single ligand-targeted nanoparticle. The dual receptor mediated endocytosis of DRT-DTX-PLGA showed a high binding affinity effect that leads to high intracellular DTX concentration and exhibited high cytotoxic properties. Thus, DRT nanoparticles have the potential to improve cancer therapy by providing selectivity over single-ligand-targeted nanoparticles.

1. Introduction

Tumor heterogeneity is a crucial feature of cancer biology and presents a complex and challenging hurdle to the development of effective cancer therapy strategies [1–3]. Intertumoral heterogeneity encompasses diverse characteristics such as cell morphology, cell signaling, cell surface markers, receptors, drug resistance, metabolism, proliferation, motility, drug resistance, angiogenesis, immunogenicity, and metastatic potential, and arises from genetic and epigenetic alterations in both cancer and tumor stromal cell [4–6]. Additionally, studies have demonstrated that different receptors are frequently upregulated in tumor cells, and drug resistance is often associated with the upregulation of alternative receptors or the switching of pathways between two receptors [7]. These factors affect the delivery efficiency of single-ligand nanomedicines, which can result in variations in the response to targeted therapy within a tumor and diminish drug efficacy [8,9]. These parameters influence the effectiveness of single-ligand nanomedicine delivery, which can lead to differences in tumor response to targeted therapy and reduce the therapeutic efficacy.

Based on the overexpression of specific receptors in tumor cells, active targeting strategies have been evolved to efficiently deliver active agents to tumor cells through receptor-mediated endocytosis. However, the efficacy of single-ligand nanoparticulate delivery systems remains limited owing to the complexity of the tumor milieu and tumor heterogeneity [9].

In recent years, dual-receptor targeting (DRT) strategies with bispecific antibodies have attracted considerable interest owing to their better tissue-penetrating properties, which have the potential to improve selectivity in tumor-targeted delivery [10]. Bispecific antibodies represent a novel approach in which two different ligands are

* Correspondence to: College of Pharmacy, Keimyung University, Daegu 42601, the Republic of Korea.
E-mail address: ysimmyung@kmu.ac.kr (S. Yook).
[1] These authors contributed equally to this work

https://doi.org/10.1016/j.biopha.2023.115023
Received 20 April 2023; Received in revised form 10 June 2023; Accepted 13 June 2023
Available online 15 June 2023

attached to a delivery system in order to target respective receptors that are overexpressed on one type of cell or different cells [11,12]. They employed Fab or scFv fragments from two different monoclonal antibodies (mAbs) connected by a peptide linker to retain the binding activity of each antibody when assembled [13]. Recently, the food drug administration (FDA) has approved three bispecific antibodies for cancer treatment: blinatumomab (Blincyto) for acute lymphoblastic leukemia, amivantamab-vmjw (Rybrevant) for non-small cell lung cancer, and tebentafusp-tebn (Kimmtrak) for uveal melanoma [14,15]. Bispecific antibodies improve binding, selectivity, and efficacy by simultaneously inhibiting two receptors or cytokines [16,17].

With the rapid increase in the use of nanotechnology for cancer management, the development of nanomedicine-based bispecific therapies could prove to be a powerful approach for increasing the selectivity and cellular uptake of tumor cells [14,18]. Nanoparticles such as poly(lactide-co-glycolide) acid (PLGA) offer flexible surface modification capabilities, providing a platform for surface conjugation with bivalent, multivalent, or multi-type antibodies that engage different targets with unique antibodies [19,20]. The use of bispecific antibodies in conjunction with nanoparticles can overcome potential instability and nonspecific binding of antibody-nanoparticle conjugates. Nanoplatforms incorporating bispecific antibodies exhibit strong binding to specific targets in addition to their small dimensions [20].

Furthermore, when two different nanoparticles and their corresponding antibodies were physically mixed, they exhibited behavior similar to that of bispecific antibody nanomedicines. However, DRT were specifically designed to have an equivalent concentration of antibodies as a single ligand-targeting nanoparticle. Such nanoparticle decorated with a single ligand promotes the accumulation of anticancer drugs to the tumor site via enhanced permeability and retention effect and can enhance cellular uptake of the nanoparticle. However, The interaction of single-ligand-targeted nanoparticles is limited due to the saturation phenomenon, attributed to the limited number of receptors on the target cell membrane. Furthermore, increasing the ligand ratio on the nanoparticle surface does not necessarily increase the intracellular accumulation of nanoparticles [21–23]. To overcome this limitation and encourage nanoparticle internalization, DRT nanoparticle have been developed to enhance tumor-targeting selectivity [24,25]. In addition, such systems can result in higher avidity and affinity than the corresponding monospecific systems [26]. The underlying idea is that the simultaneous binding of the bispecific nanoplatform to both antigens on the surface of the same cell can limit escape mechanisms and improve target selectivity through a strong avidity effect [16,26–29].

DRT nanoplatforms have been shown to differentially enrich cell surface proteins, including epidermal growth factor receptor (EGFR), programmed death-ligand1 (PD-L1), and human epidermal growth factor receptor 2 (HER2), depending on the subtype. Recently, PD-L1 expression has been shown in more than 88% of glioblastoma multiforme (GBM) [30,31], and 24–60% of non-small cell lung cancer (NSCLC) [32,33]. Furthermore, 36–40% of GBMs [34,35] and 40–89% of NSCLC exhibit EGFR gene amplification [36].

In this study, we aimed to investigate and compare the anti-cancer effects of DRT nanoplaform and compared with single antibody targeting nanoplatform. Here, we constructed a dual-targeted approach by utilizing functionalized PLGA nanoparticles with two different antibodies such as anti-EGFR antibody (panitumumab, Pmab) and anti-PD-L1 antibody and encapsulated with docetaxel (DTX), to form DRT-DTX-PLGA. Further, we developed DTX loaded PLGA (DTX-PLGA), single receptor-targeted nanoparticles such as Pmab-conjugated DTX-PLGA (Pmab-DTX-PLGA) or anti-PD-L1 conjugated DTX-PLGA (anti-PD-L1-DTX-PLGA), and a physical mixture of Pmab-DTX-PLGA and anti-PD-L1-DTX-PLGA (physical mixture (1:1)). Ligand-targeted nanoparticles have shown high targeting selectivity towards cells with overexpressed surface receptors. Bispecific antibody nanomedicines can further enhance the selectivity of targeting by simultaneously binding to two overexpressed receptors. DRT-DTX-PLGA, through its simultaneous binding to the two antigens, can cause cell death via synergistic signaling mechanisms.

2. Experimental section

2.1. Materials and methods

Resomer RG 502H poly(lactide-co-glycolide) acid (PLGA 50:50, Molecular weight (MW):54 kDa), acetone, 4′,6 diamidino-2-phenylindole (DAPI), polyvinyl alcohol (PVA), and coumarin-6 (C6), bovine serum albumin (BSA) were obtained from Sigma-Aldrich (St. Louis, MO, USA). Docetaxel (DTX) was obtained from MedChemExpress (Monmouth Junction, NJ, USA). Anti-PD-L1 antibody was purchased from BioX Cell (Lebanon, NH, USA). Pmab was acquired from Amgen Inc. (Thousand Oaks, Cambridge, USA). N-hydroxysulfosuccinimide (NHS) and 1-Ethyl-3-(3-dimethyl aminopropyl) carbodiimide hydrochloride (EDC) were acquired from TCI Co. Ltd. (Tokyo, Chuo, Japan). Pierce™ 660 nm protein assay, alexa fluor 594 anti-human IgG, and alexa fluor 488 anti-rat IgG were obtained from Thermo Scientific (Rockford, Illinois, USA). Phosphate buffer saline (PBS), RPMI 1640 medium, 10% fetal bovine serum (FBS), and streptomycin were purchased from Gibco-Invitrogen (Grand Island, NY, USA). Cy5.5-N-succinimidyl ester (Cy5.5) was obtained from Lumiprobe (Hunt Valley, Maryland, USA), and the cell counting kit (CCK-8) was obtained from Dojindo (Kumamoto, Kyushu, Japan). Calcein acetoxymethyl (calcein AM) and ethidium homodimer-1 (EthD-1) were purchased from Invitrogen (Carlsbad, CA, USA), while Vectashield mounting medium (VMM) was obtained from Vector Laboratories, Inc. (Burlingame, CA, USA). The FITC-annexin V apoptosis kit was purchased from BD Biosciences (San Diego, CA, USA). All other chemicals were of reagent grade and were used without further purification.

2.2. Cancer cell lines

The U87-MG human glioblastoma and A549 human non-small cell lung cancer (NSCLC) cell lines were obtained from the Korean Cell Line Bank (Seoul, South Korea). To cultivate the cell lines, RPMI 1640 medium supplemented with 10% FBS, 100 U/mL of penicillin, and 100 μg of streptomycin was used, and they were maintained in a 5% CO_2 atmosphere at 37 °C.

2.3. Synthesis and characterization of DTX-PLGA

DTX-PLGA was prepared with a single emulsion solvent evaporation technique. Initially, PLGA and DTX were dissolved in acetone as organic solvents for 3 h. Subsequently, the solution of drug-polymer was introduced dropwise to an aqueous solution of PVA (0.5%), and the mixture was subjected to probe-sonication at 5 amplitudes for 60 s to produce an O/W emulsion. The O/W emulsion was stirred using a magnetic stirrer for 4 h at 25 ºC until the organic phase had evaporated completely to produce nanoparticles. DTX-PLGA was collected through centrifugation at 10,000 rpm for 15 min, after which it was resuspended, washed with water, and freeze-dried [37]. Further blank PLGA was synthesized with same method as DTX-PLGA, but without DTX.

2.4. Synthesis of Pmab and anti-PD-L1 conjugated PLGA (DRT-PLGA)

To covalently attach the antibody onto the PLGA surface, the lyophilized drug containing blank PLGA was dispersed in a buffer of 0.1 M $NaHCO_3$, pH 8.5. A freshly prepared 2 mM aqueous solution of EDC was reacted to the PLGA solution with continuous stirring using a magnetic stirrer, followed by the addition of 5 mM freshly prepared NHS solution after 15 min. The mixture was then stirred magnetically for 20 min. Subsequently, the activated PLGA was treated with 300 μg (7.50 μM) of anti-PD-L1 antibody or 300 μg (2.04 μM) of Pmab to prepare anti-PD-L1-conjugated PLGA (anti-PD-L1-PLGA) and Pmab conjugated PLGA

(Pmab-PLGA), respectively. Pmab and anti-PD-L1 conjugated PLGA (DRT-PLGA) conjugates were synthesized by incubating 300 μg anti-PD-L1 antibody and Pmab (1:1) with PLGA (200 μM) at the same time. In contrast, physical mixture (1:1) was prepared by treating PLGA (200 μM) with Pmab (1.02 μM) and PLGA (200 μM) with anti-PD-L1 antibodies (3.75 μM). The reaction mixture was gently stirred for 4 h at room temperature. Ultrafiltration was used to separate excess linking reagents and soluble by-products. Finally, Pmab-PLGA, anti-PD-L1-PLGA, physical mixture (1:1), and DRT-PLGA were recovered by centrifugation at 15,000 rpm for 10 min, washed twice with distilled water, and suspended in PBS at pH 7.5 [38].

The freeze-dried blank PLGA, Pmab-PLGA, anti-PD-L1-PLGA, physical mixture (1:1), and DRT-PLGA were dispersed in distilled water (1 mg/mL). The mean nanoparticle size, polydispersity index (PDI), and zeta potential of blank PLGA, Pmab-PLGA, anti-PD-L1-PLGA, physical mixture (1:1), DRT-PLGA was determined with dynamic light scattering (DLS, Brookhaven Instruments Corp., NY, USA) equipped with a 633 nm laser and 173° backscattering angle with 15° detections angle. The laser Doppler velocimetry (electrophoretic light scattering) was used to measure zeta potential of the nanoparticles with the same instrument. Further, transmission electron microscopy (TEM; JEOL 2011, JEOL Ltd., Tokyo) was used to analyze the size and surface morphology of all formulations. To perform TEM measurements, 5 μL of each formulation was deposited onto a copper-coated grid (Ted Pella, Inc., Redding, CA, USA) separately and dried.

Additionally, the storage stability of blank PLGA, Pmab-PLGA, anti-PD-L1-PLGA, physical mixture (1:1), and DRT-PLGA conjugates was compared using DLS. All formulations were purified by ultrafiltration and suspended in distilled water and PBS (pH 7.4) for 0, 12, and 24 h. Aggregation was evaluated by determining the hydrodynamic diameter of PLGA using DLS. Then, the average particle size of each formulation was measured.

2.5. Determination of drug loading and encapsulation efficiency

The drug loading (DL) and encapsulation efficiency (EE) of nanoparticles were assessed by dissolving 10 mg of nanoparticles in 1 mL DMSO, and then diluting the solution to obtain a detectable concentration within the linear calibration range (0, 0.01, 0.1, 0.25, 0.5, 1, 5, 10, 25, and 50 μg/mL). The UV absorbance of the solution was measured at 275 nm using a microplate reader. To estimate the mass of DTX loaded into PLGA, the mass of DTX used in the DTX-PLGA formulation was subtracted from the mass of DTX in the supernatant. The DL and EE of the active agents were calculated using the following equations:

$$EE(\%) = \left(\frac{\text{Total DTX mass} - \text{unloaded DTX}}{\text{Total DTX mass}}\right) \times 100$$

$$DL(\%) = \left(\frac{\text{Total DTX mass} - \text{unloaded DTX}}{\text{Total PLGA mass}}\right) \times 100$$

2.6. Determination of surface chemistry of DTX-PLGA

The surface structural characteristics of DTX-PLGA in the solid state were analyzed by fourier-transform infrared spectroscopy (FT-IR, Nicolet iS10; Thermo Scientific Inc., Waltham, MA, USA). Samples of freeze-dried PLGA, DTX, DTX-PLGA, and a physical mixture of PLGA together with DTX powder were scanned in the infrared range of 400–4000 cm^{-1} to obtain spectra.

2.7. Evaluation of in vitro drug release

The *in vitro* release of DTX from DTX-PLGA was performed following previously described protocols [37,39]. Briefly, freeze-dried DTX-PLGA (5 mg) was dispersed in a centrifuge tube containing 10 mL of PBS (containing 0.1% v/v Tween 80, pH 7.4, and pH 5.5). The tube was then placed into an orbital shaker incubator at 120 rpm at 37 °C. At fixed time intervals, the tubes were removed and centrifuged for 10 min at 15, 000 rpm. The supernatant was collected and transferred to a test tube for UV absorbance measurements. The remaining pellet was re-dispersed in fresh PBS and returned to the shaker for subsequent measurements. Quantification was performed using a calibration curve of DTX in the corresponding buffer solutions.

2.8. Evaluation of conjugation efficiency of antibodies on PLGA

The conjugation efficiency (CE) of Pmab and the anti-PD-L1 antibody to PLGA was investigated using a standard protein assay kit. To achieve this, Pierce™ reagent (150 μL) was mixed to 1 μL of the Pmab-PLGA, anti-PD-L1-PLGA, physical mixture (1:1), or DRT-PLGA dispersion and incubated for 10 min at a dark place. Then, microplate reader (Infinite™ M200 PRO, Tecan, Msing Inf, Switzerland) was used to measure the UV absorbance at 660 nm. The results were compared to a standard calibration curve of BSA solution in the concentration range of 0, 125, 250, 500, 750, 1000, 1500, and 2000 μg/mL. The absorbance of cetuximab was measured at 280 nm. The mass of the PLGA-conjugated antibody was estimated by subtracting the mass of the antibody used in the formulation from that of the supernatant. The total antibody CE% on the PLGA was calculated as follows:

$$CE\% = \left(\frac{\text{Mass of antibody conjugated on PLGA}}{\text{Mass of antibody used in this formulation}}\right) \times 100$$

2.9. Evaluation of EGFR and PD-L1 receptor expression

The expression of EGFR and PD-L1 receptors in U87-MG and A549 cells was measured using flow cytometry (FACS). Firstly, U87-MG and A549 cells were seeded at a density of 2×10^5 cells/well in 6-well plates and allowed to grow overnight. The cells were then trypsinized, blocked with 2% FBS and 0.5% BSA in PBS, and incubated with either anti-PD-L1 antibodies or Pmab for 2 h at 25 °C. After rinsing with PBS, the cells were incubated with 8 μg/mL of Alexa Fluor 488 anti-rat IgG and Alexa Fluor 594 anti-human IgG at 4 °C for 1 h. Then the cells were dispersed in a FACS staining buffer (PBS containing 0.05% sodium azide and 0.1% BSA) and analyzed by FACS. The relative median fluorescence intensities (RMFI) of the cells were evaluated and compared with those of the controls. The RMFI for each cell line was calculated by the formula [40]:

$$RMFI(\%) = \frac{\text{Median fluorescence intensity (Pmab) or (anti} - \text{PD} - \text{L1 Ab)}}{\text{Median fluorescence intensity(control)}}$$

The expression of EGFR and PD-L1 was determined using confocal laser scanning microscopy (CLSM, Carl Zeiss LSM5; Carl Zeiss Inc., Germany)). U87-MG and A549 cells (5×10^5 cells/well) were seeded on cover glass slips in 6-well plates and cultured overnight at 37 °C. The cells were further incubated with 10 μg/mL of Pmab and anti-PD-L1 antibodies for 2 h. Subsequently, cells were fixed with 4% paraformaldehyde, rinsed, and incubated with 8 μg/mL of Alexa Fluor 488 anti-rat IgG to bind to Pmab, Alexa Fluor 594 anti-human IgG to bind to anti-PD-L1 antibody. Cells were incubated with DAPI (10 μg/mL) for 15 min to stain the nuclei. Then, VMM was used to mount the slides and sealed. Finally, images of cells were obtained using a CLSM.

2.10. Immunoreactivity assay

Briefly, 2×10^5 U87-MG and A549 cells were cultured in 6-well plates. Following the trypsinization, the cells were blocked with 2% FBS and 0.5% BSA in PBS. Subsequently, they were incubated with NT-PLGA, Pmab-PLGA, anti-PD-L1-PLGA, physical mixture (1:1), or DRT-PLGA at 4 ℃ for 4 h. After washing with PBS, cells were incubated with 8 μg/mL of Alexa Fluor 488 anti-rat IgG and Alexa Fluor 594 anti-

human IgG at 4 °C for 1 h, rinsed, and dispersed in FACS staining buffer and analyzed by FACS. To compare the immunoreactivities of NT-PLGA, Pmab-PLGA, anti-PD-L1-PLGA, physical mixture (1:1), and DRT-PLGA, CLSM was also used. U87-MG and A549 cells (5×10^5 cells/well) were plated on cover glass slips in 6-well plates and cultured overnight at 37 °C. The cells were then further incubated with NT-PLGA, Pmab-PLGA, PD-L1-PLGA, physical mixture (1:1), or DRT-PLGA 4 ºC for 4 h. Finally, cells were fixed with 4% paraformaldehyde, washed, and then stained with DAPI (10 μg/mL). The slides were mounted in VMM and sealed. Finally, CLSM was used to obtain the image of cells.

2.11. Cellular uptake of DRT-PLGA

To evaluate the cellular uptake of various types of nanoparticles loaded with C6, U87-MG and A549 cells (5×10^5 cells/well) were seeded in 6-well plates and cultured overnight at 37 °C. After removing the medium, the cells were incubated for 6 h with non targeted C6 loaded PLGA nanoparticles (NT-C6-PLGA), Pmab- conjugated C6-PLGA (Pmab-C6-PLGA), anti-PD-L1 conjugated C6-PLGA (anti-PD-L1-C6-PLGA), physical mixture of Pmab-C6-PLGA and anti-PD-L1-C6-PLGA (physical mixture (1:1)), or Pmab and anti-PD-L1 conjugated C6-PLGA (DRT-C6-PLGA) (equivalent concentration of C6, 4 μg/mL of an aqueous solution of PLGA). The cells were then trypsinized, rinsed three times with PBS, and analyzed using FACS to quantify cellular uptake.

Moreover, the qualitative analysis of cellular uptake was determined using CLSM. Briefly, U87-MG and A549 cells (5×10^5 cells/well) were seeded on cover glass slips in 6-well plates and cultured overnight for 24 h at 37 °C. After removing the medium, the cells were then incubated for 6 h with NT-C6-PLGA, Pmab-C6-PLGA, anti-PD-L1-C6-PLGA, physical mixture (1:1), or DRT-C6-PLGA (equivalent concentration of C6, 4 μg/mL of an aqueous solution of PLGA). The cells were subsequently rinsed with PBS, fixed with 4% paraformaldehyde, and incubated with DAPI (10 μg/mL) to stain the nuclei. Finally, the slides were mounted in VMM and sealed, and images were captured using CLSM [41].

2.12. In vitro cytotoxicity assay

The IC_{50} value of DTX was evaluated using a CCK-8 assay. Specifically, U87-MG and A549 cells (1×10^4 cells/well) were seeded in a 96-well plate and incubated overnight at 37 °C. The cells were incubated with DTX (0, 0.01, 0.1, 0.5, 1, 2.5, 10, or 25 μg/mL of DTX) for 8 h. After incubation, the cells were washed with PBS and incubated for an additional 24 h. Finally, 10 μL of CCK-8 solution was added to each well, and the cells were incubated at 37 °C for 4 h. The absorbance of formazan was measured at 450 nm using an Infinite M200 PRO microplate reader (Tecan, Msing Inc., Switzerland).

In addition, to assess the *in vitro* cytotoxicity, U87-MG and A549 cells (1×10^4 cells/well) were seeded in a 96-well plate and incubated overnight at 37 °C. Then, cells were incubated with DTX, NT-DTX-PLGA, Pmab-DTX-PLGA, anti-PD-L1-DTX-PLGA, physical mixture (1:1), or DRT-DTX-PLGA at equivalent concentrations of DTX (0.5- μg/mL) for 8 h. After incubation, the cells were washed with PBS and incubated for an additional 24 h. Finally, CCK-8 solution (10 μL) was added to each well, and the cells were incubated at 37 °C for 4 h. The absorbance of formazan at 450 nm was determined using an Infinite M200 PRO microplate reader.

To evaluate membrane integrity, calcein-AM, and EthD-1 were used. Briefly, 2×10^5 U87-MG and A549 cells were cultured in a 12-well plate and incubated overnight. Then, DTX, NT-DTX-PLGA, Pmab-DTX-PLGA, anti-PD-L1-DTX-PLGA, physical mixture (1:1), or DRT-DTX-PLGA (concentration equivalent 0.5 μg/ mL of DTX) was added to the cells. After 24 h incubation, calcein-AM (2 μM) and EthD-1 (4 μM) were used to stain live and dead, respectively, and incubated for 30 min. Cells were subsequently rinsed with PBS and added fresh media. Finally, images were captured using a fluorescence microscope (IX71, Olympus Tokyo, Japan).

2.13. Apoptosis assay

To evaluate the apoptotic effects of DRT-DTX-PLGA on U87-MG and A549 cells, a FITC-Annexin V apoptosis kit was used. Initially, U87-MG and A549 cells (2×10^5 cells/well) were seeded in 12-well plates and incubated at 37 °C overnight. Subsequently, the cells were treated with different formulations, including DTX, NT-DTX-PLGA, Pmab-DTX-PLGA, anti-PD-L1-DTX-PLGA, physical mixture (1:1), or DRT-DTX-PLGA (concentration equivalent 0.5 μg/mL of DTX). Following a 24 h incubation, the cells were rinsed with PBS, trypsinized the cells from the well surfaces, and redispersed in 500 μL annexin V binding buffer. Then, the cells were incubated with 5 μL of FITC-annexin and propidium iodide (PI) for 30 min to determine apoptotic cell death. Lastly, the cells were distributed in an annexin V-binding buffer and analyzed by FACS.

2.14. Statistical analysis

Unpaired Student's t-tests were performed for intergroup comparisons. Data were expressed as means ± SD for triplicates. The level of statistical significance differences was set as P values of * $**p < 0.001$, * $*p < 0.01$, and $*p < 0.05$.

3. Results

3.1. Preparation and characterization of DRT-DTX-PLGA

We utilized the single-emulsion solvent evaporation method to develop DTX-PLGA and DRT-DTX-PLGA (Fig. 1A and 1B, respectively). The mean particle sizes of blank PLGA, Pmab-PLGA, anti-PD-L1-PLGA, physical mixture (1:1), and DRT-PLGA were 108.2 ± 2.3, 123.3 ± 1.5, 122.1 ± 1.7, 122.2 ± 1.6 and 124.2 ± 1.1 nm, respectively (Fig. 2A) with PDI values of 0.11 ± 0.02, 0.14 ± 0.02, 0.16 ± 0.02, 0.20 ± 0.02, and 0.18 ± 0.02, respectively (Fig. 2A). Furthermore, the surface charge of blank PLGA-NPs, Pmab-PLGA, anti-PD-L1-PLGA, physical mixture (1:1), and DRT-PLGA were − 38.7 ± 2.1, − 28.9 ± 1.8, − 27.4 ± 2.4, − 28.1 ± 2.7, and − 24.6 ± 3.1 mV respectively (Fig. 2B). TEM images confirmed that blank PLGA showed a spherical morphology, and the conjugation of Pmab and anti-PD-L1 to the PLGA surface was further verified (Fig. 2C). A thin outer layer on PLGA coated with Pmab and anti-PD-L1 was observed in TEM images (Fig. 2C). The DL% and EE% of DTX were 2.5 ± 0.8%. 71.9 ± 1.2%. The optimal DTX concentration of 10 mg/mL was used in subsequent experiments.

To assess the physical stability of blank PLGA, Pmab-PLGA, anti-PD-L1-PLGA, physical mixture (1:1), and DRT-PLGA, we observed the particle size of the freeze-dried form of the formulations at storage temperatures of 4 °C over 0, 12 and 24 h (Fig. 2D). The hydrodynamic diameter particle sizes of all formulations showed excellent physical stability, with no significant difference in particle size up to 24 h.

To characterize the chemical functionalization of DTX-PLGA, FT-IR spectra were compared with those of the individual ingredients used in the preparation of DTX-PLGA and the physical mixture of DTX and PLGA (Fig. 2E). PLGA showed a major characteristic peak at 1752 cm^{-1} (COOH vibration) [19,42]. The major peaks at 1752 (C═O) and 1170 (C–O) cm^{-1} are characteristic stretching vibrations and bonds of PLGA. The spectrum of free DTX showed two characteristic absorption peaks at 3464 (O-H), 1704 (C═O) of ester, 1494 (benzene ring), and 1370 (C–H stretch) cm^{-1}. This result is consistent with those reported by Li and Zuo [43] and Kulhari et al. [44]. In the study reported by Li and Zuo [43], FT-IR spectra of DTX were obtained at 3462 (O–H stretch), 1465 (benzene ring), and 1344 (C–H stretch) cm^{-1}. The major peaks of DTX-PLGA appeared at 2880 (C–H stretch), 1762 (C═O stretch), 1468 (benzene ring), 1341 (O–H stretch), and 1097 (C–O stretch) cm^{-1}. The C═O stretching shifted from 1704 (DTX) to 1762 cm^{-1} (DTX-PLGA). The benzene ring stretching shifted from 1494 (DTX) to 1468 cm^{-1} (DTX-PLGA). The C–H stretching shifted from 1370 (DTX) to 1341 cm^{-1} (DTX-PLGA). These peak shifts indicated interactions between DTX and

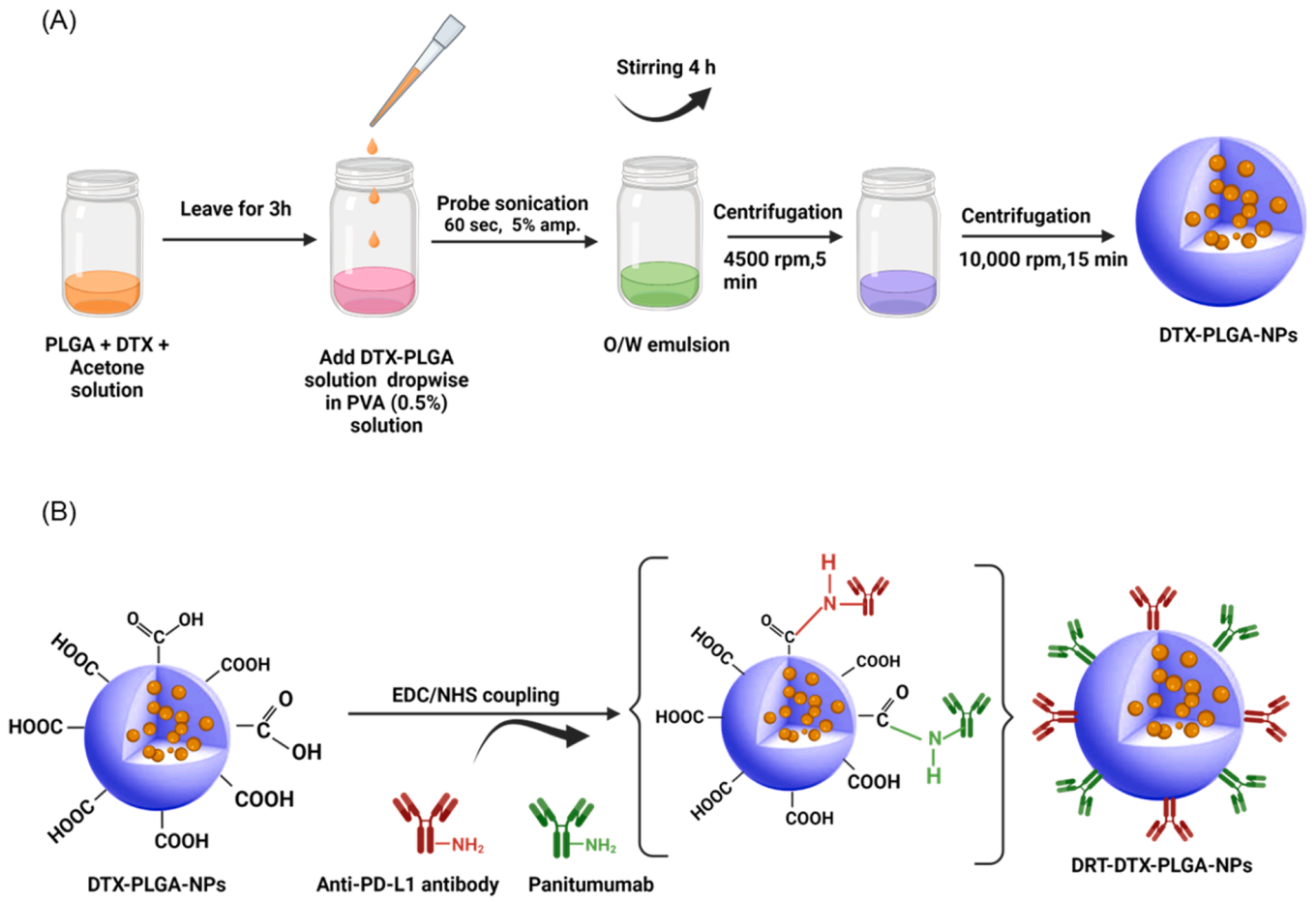

Fig. 1. Schematic illustration of synthesis of DTX-PLGA and DRT-DTX-PLGA. (A) DTX-PLGA were synthesized by the single emulsion solvent evaporation method, (B) DRT-DTX-PLGA were developed by conjugating anti-PD-L1 and Pmab on surface of DTX-PLGA via EDC/NHS coupling chemistry.

the polymer in the PLGA formulations. The spectrum of the physical mixture of DTX and PLGA showed the major peaks of PLGA and DTX, although some superposition occurred.

Fig. 2F demonstrated that the desired CE% was achieved by conjugating Pmab (150 μg/mL) and anti-PD-L1 (150 μg/mL) onto the surface of PLGA to produce Pmab-PLGA, anti-PD-L1-PLGA, physical mixture (1:1), and DRT-PLGA. The maximum CE% of DRT-PLGA was 76.2 ± 6.2 %. Additionally, as illustrated in Fig. 2G, the concentration of conjugated antibodies on PLGA for DRT-PLGA was found to be 3.3 ± 0.8 μg/mL (Pmab) and 3.4 ± 0.6 μg/mL (anti-PD-L1) in 1 mg of PLGA.

3.2. *In vitro drug release study*

We determined the *in vitro* release profile of DTX in DTX-PLGA for up to 144 h in two physiological media: PBS with basic pH 7.4 and acidic pH 5.5. The patterns of drug release from PLGA were evaluated at basic pH (mimicking physiological conditions) to compare the release patterns under acidic pH (mimicking tumor microenvironment). As shown in Fig. 2H, the cumulative release of DTX from DTX-PLGA in acidic media was 60.5 ± 6.5% and 30 ± 7.5%, respectively, after 144 h. Furthermore, PLGA is easily dissolved in acidic media, resulting in high drug release in the acidic environment of the tumor site compared to the physiological pH, leading to increased anti-tumor efficacy and reduced adverse effects on healthy tissue.

3.3. *Characterization of cellular expression of EGFR and PD-L1 receptors*

Quantitative analysis of cellular expression of EGFR and PD-L1 receptors on U87-MG and A549 was analyzed by FACS (Fig. 3A). U87-MG cells exhibited a 2.2- fold higher fluorescence signal for PD-L1 than that of the A549 cell line. Conversely, A549 cells displayed a 21.1- fold higher fluorescence signal for EGFR than that of U87-MG cells. Furthermore, the qualitative data obtained using CLSM supported the quantitative data of receptor expression in U87-MG and A549 cell lines (Fig. 3B). Green fluorescence represents EGFR expression and red fluorescence represents PD-L1 expression. U87-MG and A549 cell lines showed high levels of PD-L1 and EGFR receptors, respectively.

3.4. *Immunoreactivity of DRT-PLGA*

The immunoreactivity of DRT-PLGA was evaluated in U87-MG and A5649 cell lines by FACS and compared with that of Pmab-PLGA and anti-PD-L1-PLGA (Figs. 4A and 5B), respectively. In U87-MG cell line (Fig. 4A), the RMFI of DRT-PLGA and Pmab-PLGA were significantly similar (***$p < 0.001$). Similarly, in A549 cells (Fig. 4B), the RMFI of DRT-PLGA was similar to that of anti-PD-L1-PLGA (***$p < 0.001$). The quantitative analysis of immunoreactivity was further supported by a qualitative analysis performed using CLSM.

In Fig. 4C and 4D, green fluorescence represents the immunogenic properties of Pmab, whereas red fluorescence represents the immunogenic properties of anti-PD-L1. The intensity of green fluorescence in the Pmab-PLGA-treated U87-MG (Fig. 4C) and A549 (Fig. 4D) cell lines was similar to that of DRT-PLGA. Similarly, the red fluorescence intensity in anti-PD-L1-PLGA treated U87-MG (Fig. 4C) and A549 (Fig. 4D) cell lines was similar to that of the DRT-PLGA. These results suggest that the immunoreactivity of Pmab and anti-PD-L1 was retained in the DRT-PLGA formulation.

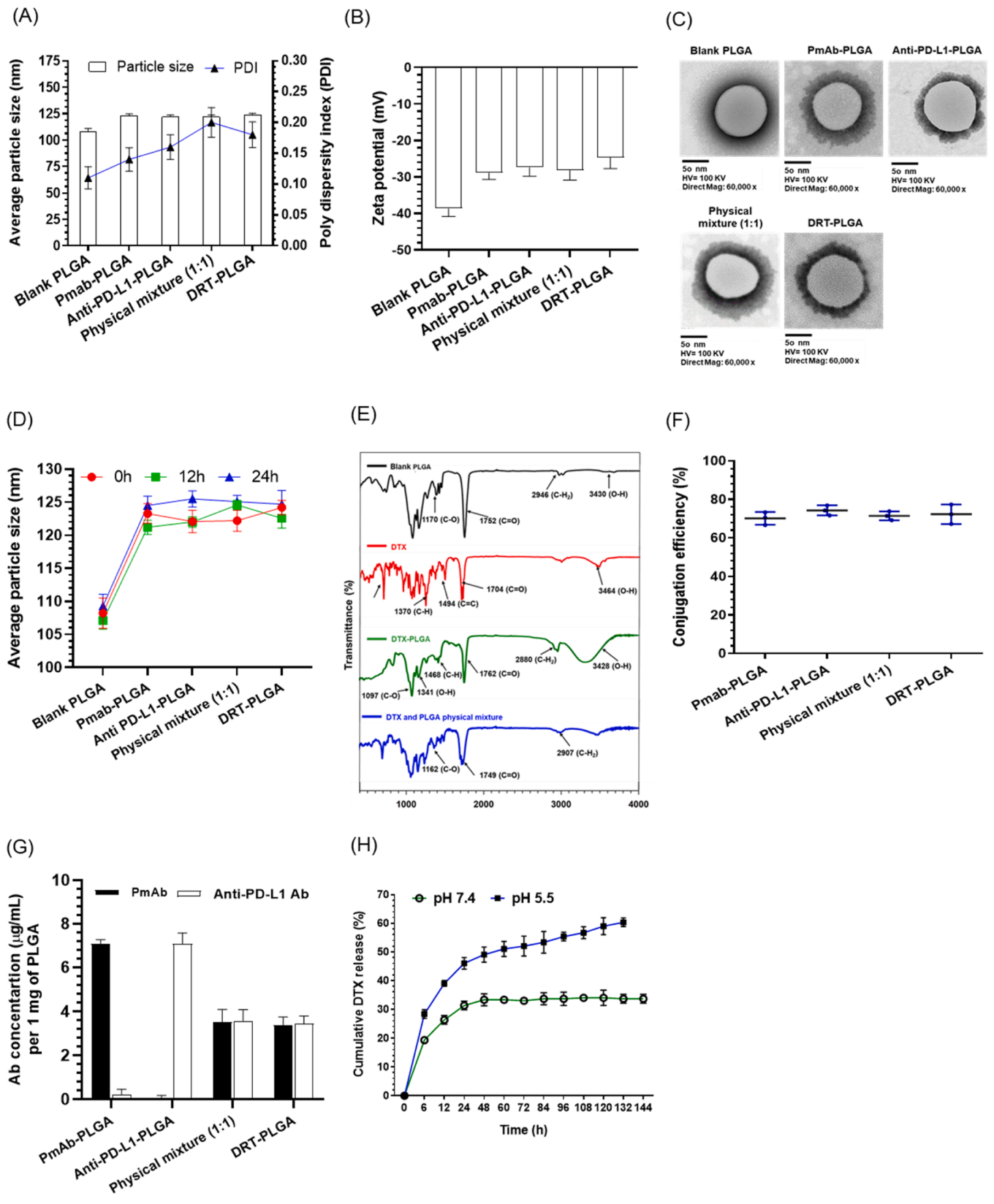

Fig. 2. Characterization of DRT-DTX-PLGA. (A) Determination of average particle size and PDI of blank PLGA, Pmab-PLGA, anti-PD-L1-PLGA, physical mixture (1:1), and DRT-PLGA using DLS. (B) Zeta potential of blank PLGA, Pmab-PLGA, anti-PD-L1-PLGA, physical mixture (1:1), and DRT-PLGA. (C) TEM image of blank PLGA, Pmab-PLGA, anti-PD-L1-PLGA, and Pmab-PLGA-PD-L1 conjugate reacted with 5-nm-gold labeled IgG. (D) Stability of PLGA, Pmab-PLGA, anti-PD-L1-PLGA, physical mixture (1:1), and DRT-PLGA incubated with PBS at 4ºC using DLS measurement. (E) FT-IR spectrum of DTX, PLGA, DTX-PLGA, and physical mixture of DTX and PLGA powder. (F) Antibody conjugation efficiency of Pmab-PLGA, anti-PD-L1-PLGA, physical mixture (1:1), and DRT-PLGA. (G) Determination of antibodies concentration on the surface of PLGA. (H) *In vitro* DTX release from DTX-PLGA in PBS, pH 7.4 and pH 5.5.

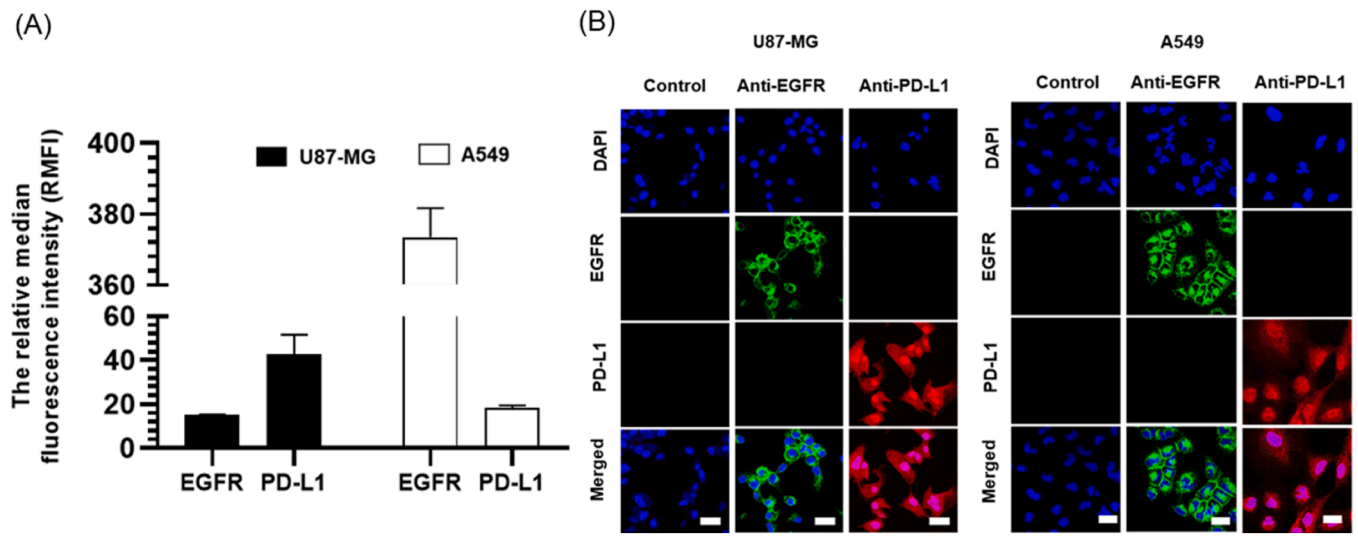

Fig. 3. Expression of EGFR and PD-L1. (A) FACS results for the fluorescence of Pmab and anti-PD-L1 antibodies associated with U87-MG and A549 cells. (B) CLSM images of U87-MG and A549 cells treated with Pmab and anti-PD-L1 antibodies. Cells were incubated with Alexa Fluor 488-anti human IgG (green) and Alexa Fluor 594-anti rat IgG (red), which visualize Pmab and anti-PD-L1 antibodies, respectively. Cell nuclei were stained with DAPI (blue). Scale bar: 25 μm.

3.5. Cellular uptake of DRT-PLGA

A quantitative analysis was conducted to evaluate the intracellular uptake of DRT-C6-PLGA in U87-MG and A549 cells using FACS (Fig. 5A and B). As illustrated in the Fig. 5A, the C6 fluorescence intensities of U87-MG cells treated with DRT-C6-PLGA were significantly increased by 9.2-fold (***$p < 0.01$), 2.4-fold (***$p < 0.001$), 3.1-fold (***$p < 0.001$), and 1.6-fold (**$p < 0.001$) compared to NT-C6-PLGA, Pmab-C6-PLGA, anti-PD-L1-C6-PLGA, and physical mixture (1:1), respectively. Similarly, in Fig. 5B, the C6 fluorescence intensities of A549 cells treated with DRT-C6-PLGA were also significantly increased by 12.0-fold (***$p < 0.01$), 2.7-fold (***$p < 0.001$), 3.5-fold (***$p < 0.001$), and 1.9-fold (**$p < 0.001$) compared to NT-C6-PLGA, Pmab-C6-PLGA, anti-PD-L1-C6-PLGA, and physical mixture (1:1), respectively.

The CLSM was employed to perform a qualitative analysis of DRT-C6-PLGA internalization in U87-MG (Fig. 5C) and A549 cell lines (Fig. 5D). The U87-MG cell line exhibited the highest fluorescence intensity for C6 in the DRT-C6-PLGA treated group, followed by the physical mixture (1:1). Single receptor-targeted nanoparticles (Pmab-C6-PLGA and anti-PD-L1-C6-PLGA) showed greater uptake than the NT-C6-PLGA treated group, and this was supported by receptor-mediated endocytosis. Similarly, in the A549 cell line, higher cellular internalization of nanoparticles was observed in DRT-C6-PLGA, followed by the physical mixture (1:1), Pmab-C6-PLGA, and anti-PD-L1-C6-PLGA. However, the Pmab-C6-PLGA treated A549 cell line showed a higher fluorescence intensity of C6 than the Pmab-C6-PLGA treated U87-MG cell line, due to the higher expression of EGFR in A549 cells compared to the U87-MG cells. Moreover, the anti-PD-L1-C6-PLGA treated U87-MG cell line showed a higher fluorescence intensity of C6 than the anti-PD-L1-C6-PLGA treated A549 cell line, because of the higher expression of PD-L1 in U87-MG cells compared to A549 cells.

3.6. In vitro cytotoxicity assay

The cell cytotoxicity assay was conducted on U87-MG and A549 cell lines by incubating with various concentrations of DTX (0, 0.01, 0.1, 0.5, 1, 2.5, 10, or 25 μg/mL of DTX) for 8 h. We observed that the IC_{50} values of the inhibitors were markedly affected by highly dependent on DTX concentration in both cell lines. As depicted in the Fig. 6A and 6B, the IC_{50} values of free DTX were 0.5 μg/mL for U87-MG and A549 cells. Furthermore, we assessed the cytotoxicity of DTX, NT-DTX-PLGA, Pmab-DTX-PLGA, anti-PD-L1-DTX-PLGA, physical mixture (1:1), and DRT-DTX-PLGA at 24 h in both U87-MG (Fig. 6C) and A549 (Fig. 6D) cells. The NT-DTX-PLGA at an equivalent concentration of 0.5 μg/mL reduced the cell viability in both U87-MG (55.6 ± 5.2%) and A549 (88.4 ± 4.9%) cell lines. The cell viability after the treatment of Pmab-DTX-PLGA, anti-PD-L1-DTX-PLGA, and physical mixture (1:1) in the U87-MG cell line was 70.1 ± 7.8%, 70.3 ± 6.1%, and 44.6 ± 3.4%, respectively. Similarly, the cell viability after the treatment of Pmab-DTX-PLGA, anti-PD-L1-DTX-PLGA, and physical mixture (1:1) in the A549 cell line was 60.3 ± 5.9%, 83.3 ± 8.2%, and 40.6 ± 7.3%, respectively. Moreover, a notable reduction in cell viability was observed when U87-MG (25.1 ± 5.3%) and A549 (20.6 ± 7.8%) cells were treated with DRT-DTX-PLGA compared to other formulations. The viability of U87-MG cells treated with DRT-DTX-PLGA was significantly diminished by 2.2-fold (**$p < 0.01$), 2.7-fold (***$p < 0.001$), 2.8-fold (***$p < 0.001$), and 1.7-fold (**$p < 0.001$) compared to DTX, Pmab-DTX-PLGA, anti-PD-L1-DTX-PLGA, and physical mixture (1:1), respectively. Similarly, the viability of the A549 cell line treated with DRT-DTX-PLGA was significantly diminished by 4.2-fold (**$p < 0.01$), 2.9-fold (**$p < 0.001$), 4.1-fold (***$p < 0.001$), and 1.9-fold (**$p < 0.001$) compared to DTX, Pmab-DTX-PLGA, anti-PD-L1-DTX-PLGA, and physical mixture (1:1), respectively. These results suggest that in both cell lines, the cytotoxic effects of DRT-DTX-PLGA were significantly higher than NT-DTX-PLGA and free DTX.

The cellular cytotoxicity was qualitatively evaluated using a live-dead assay (Fig. 6E and 6F). Incubation with NT-DTX-PLGA reduced the number of live cells, as evidenced by the decrease in green fluorescence, and increased the number of dead cells, as shown by the red color in both U87-MG (Fig. 6E) and A549 (Fig. 6F) cell lines. Additionally, incubation with Pmab-DTX-PLGA and anti-PD-L1-DTX-PLGA increased the number of dead cells while decreasing the number of viable cells in both cell lines. Importantly, DRT-DTX-PLGA exhibited a significant cytotoxicity effect with less viable cells, which could be attributed to its bispecific targeting property in both U87-MG and A549 cell lines, resulting in superior therapeutic effect compared to Pmab-DTX-PLGA and anti-PD-L1-DTX-PLGA.

3.7. Apoptosis assay

The apoptotic effects of various formulations, including DTX, NT-DTX-PLGA, Pmab-DTX-PLGA, anti-PD-L1-DTX-PLGA, the physical mixture (1:1), and DRT-DTX-PLGA were assessed using an annexin V/PI

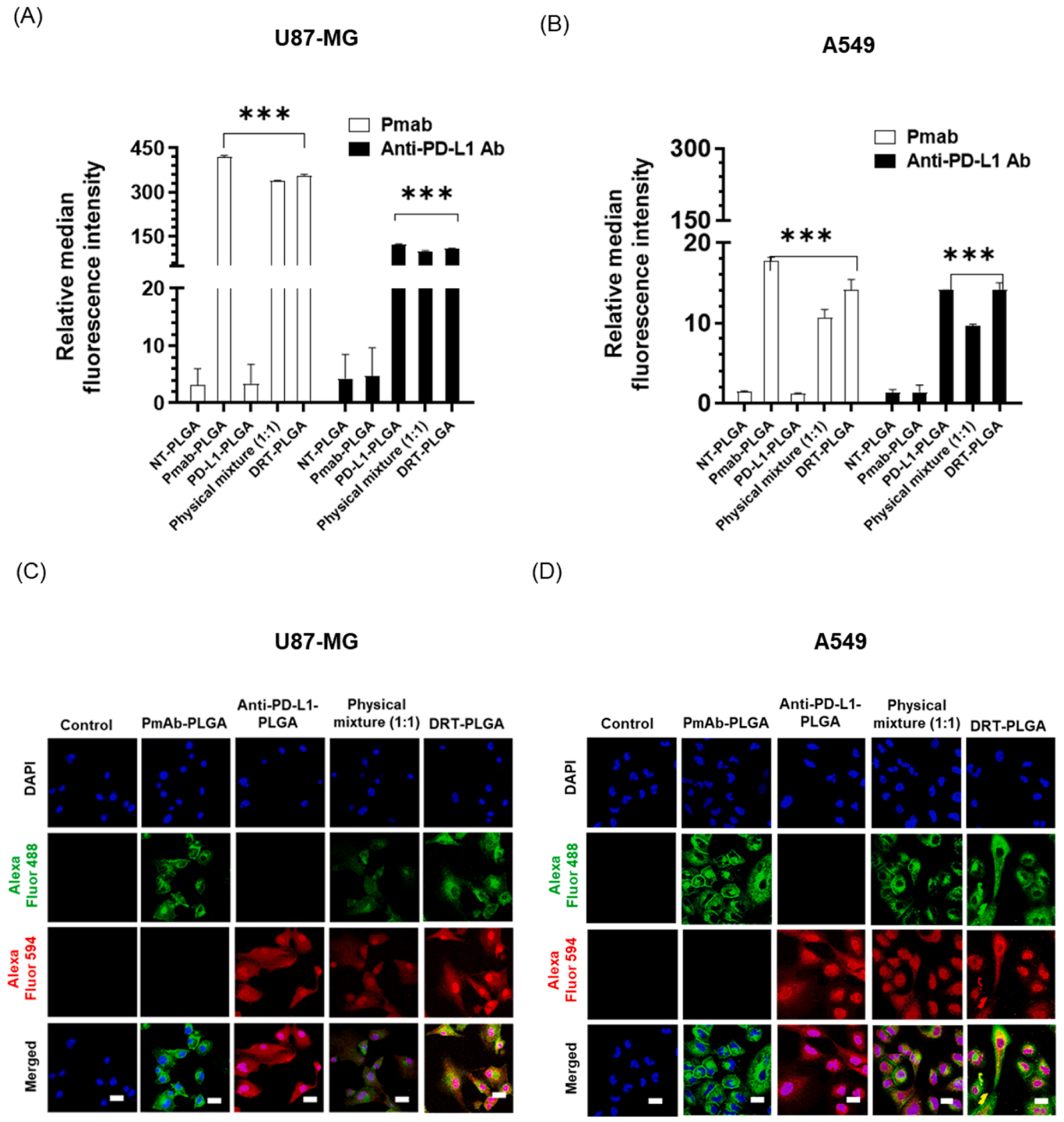

Fig. 4. Immunoreactivity of DRT-PLGA in U87-MG cells. FACS results for the fluorescence of Pmab-PLGA, anti-PD-L1-PLGA, physical mixture (1:1), and DRT-PLGA associated with (A) U87-MG cells and (B) A549 cells. CLSM images of (C) U87-MG cells and (D) A549 cells treated with Pmab-PLGA, anti-PD-L1-PLGA, physical mixture (1:1), and DRT-PLGA. Cells were incubated with Alexa Fluor 488-anti human IgG (green) and Alexa Fluor 594-anti rat IgG (red), which visualize Pmab and anti-PD-L1 antibodies, respectively. DAPI (blue) was used to stain cell nuclei. Scale bar: 25 μm.

kit in both cell line U87-MG (Fig. 7A) and A549 (Fig. 7B). The results indicated that free DTX induced apoptosis in both U87-MG (31.6 ± 4.3% apoptosis) and A549 (31.4 ± 2.3% apoptosis) cell lines. Furthermore, Pmab-DTX-PLGA and anti-PD-L1-DTX-PLGA treatments resulted in enhanced apoptotic cell death in both U87-MG (21.9 ± 5.1%, and 21.0 ± 3.1%, respectively) and A549 (30.6 ± 3.6% and 14.5 ± 2.7% respectively) cell lines. Physical mixture (1:1) treated cells showed higher apoptotic cell percentages in both U87-MG (32.3 ± 2.9%) and A549 (32.3 ± 4.3%) cell lines. The percentages of apoptotic cells in U87-MG and A549 cell lines after DRT-DTX-PLGA treatment were significantly higher (72.0 ± 6.1% and 78.7 ± 4.6%, respectively) than in other formulations. Statistically, after DRT-DTX-PLGA treatment, the apoptotic cells percentage of U87-MG was significantly increased by 2.2-fold (**$p < 0.01$), 3.1-fold (***$p < 0.001$), 3.4-fold (***$p < 0.001$), and 2.2-fold (**$p < 0.001$) after DRT-DTX-PLGA treatment, compared to DTX, Pmab-DTX-PLGA, anti-PD-L1-DTX-PLGA, and physical mixture (1:1), respectively. Similarly, after treatment with DRT-DTX-PLGA, the apoptotic cells percentage of A549 was also

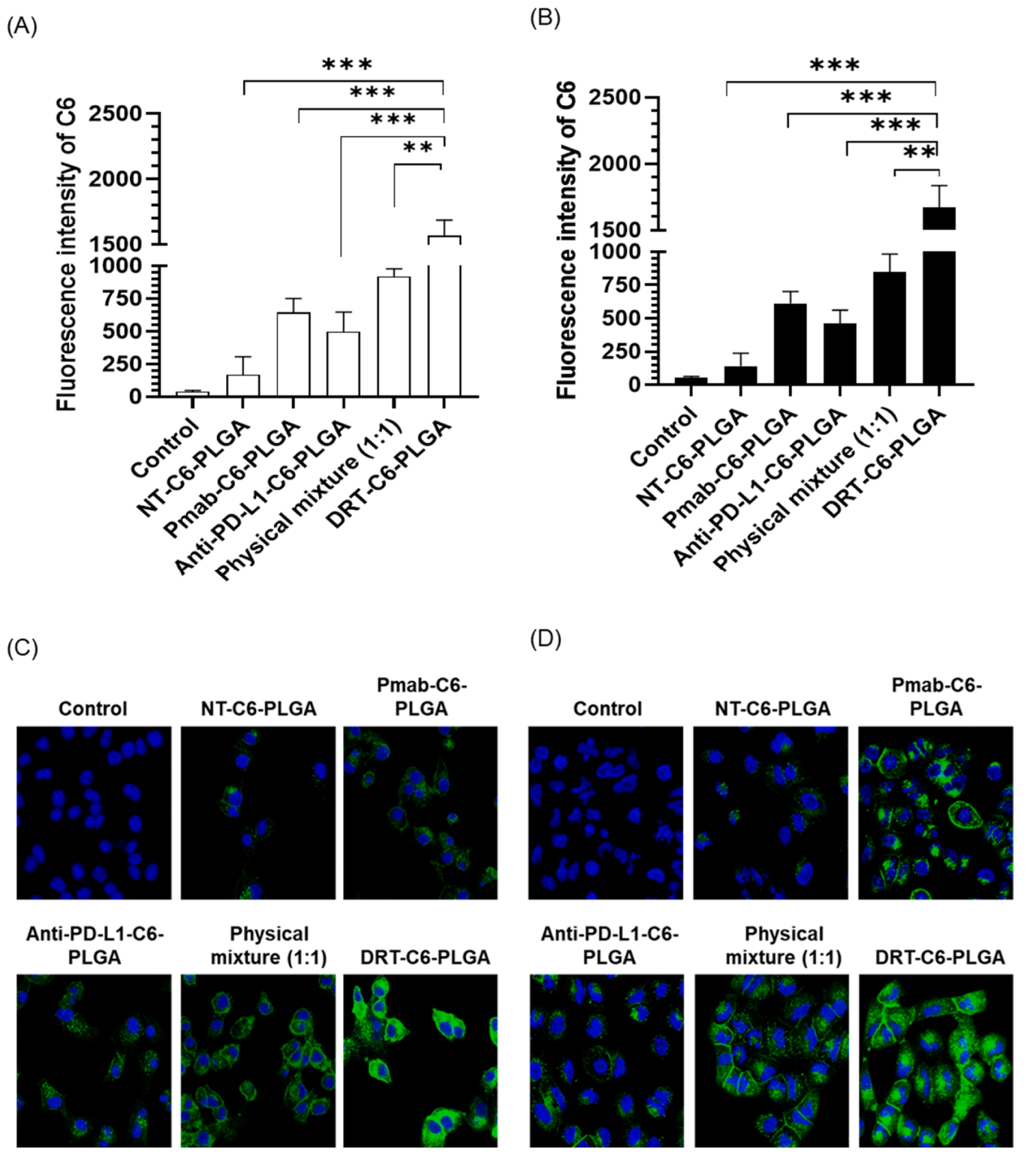

Fig. 5. Cellular uptake of DRT-C6-PLGA. (A) FACS analysis for the cellular uptake of DRT-C6-PLGA in U87-MG cells and (B) FACS analysis for the cellular uptake in A549 cells. (C) CLSM images for the determination of cellular uptake in U87-MG and A549 cells treated with NT-C6-PLGA, Pmab-C6-PLGA, anti-PD-L1-C6-PLGA, physical mixture (1:1), and DRT-C6-PLGA. DAPI (blue) was used to stain cell nuclei. Scale bar: 400 μm.

significantly increased by 2.5-fold (**$p < 0.01$), 2.5-fold (***$p < 0.001$), 5.4-fold (***$p < 0.001$), and 2.4-fold (**$p < 0.001$) compared to Statistically, the apoptotic percentage of U87-MG cell was significantly increased by 2.2-fold (**$p < 0.01$), 3.1-fold (***$p < 0.001$), 3.4-fold (***$p < 0.001$), and 2.2-fold (**$p < 0.001$) after DRT-DTX-PLGA treatment, compared to DTX, Pmab-DTX-PLGA, anti-PD-L1-DTX-PLGA, and physical mixture (1:1), respectively.

4. Discussion

PLGA nanoparticles have been widely utilized for the delivery of cytotoxic drugs to tumors using the enhanced permeability retention

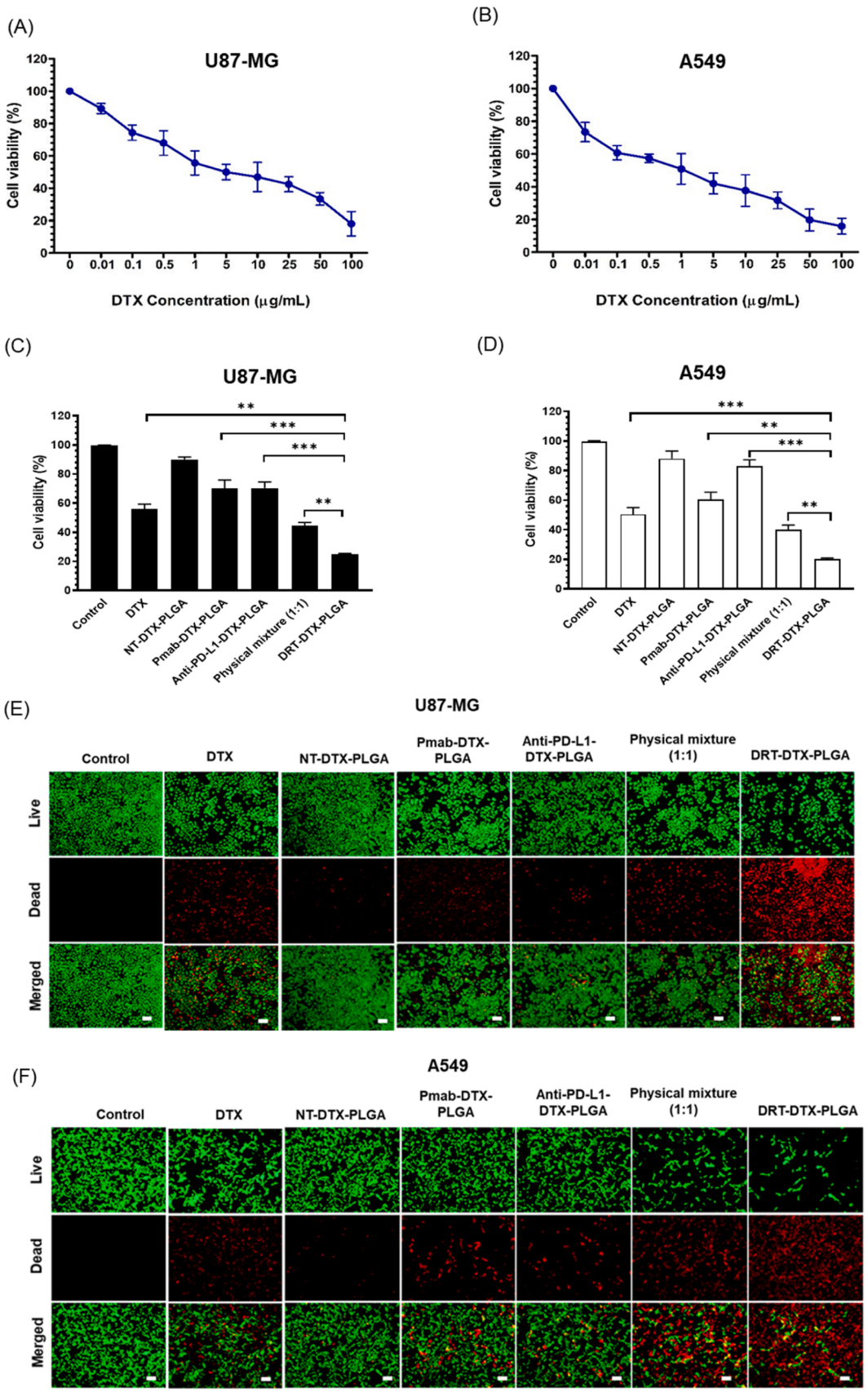

Fig. 6. Determination of *in vitro* cell viability. (A) U87-MG and (B) A549 cells were transfected to different concentrations of DTX (0, 0.01, 0.1, 0.5, 1, 2.5, 10, and 25 μg/mL) for 24 h. *In vitro* viability of (C) U87-MG and (D) A549 cells exposed to DTX, NT-DTX-PLGA, Pmab-DTX-PLGA, anti-PD-L1-DTX-PLGA, physical mixture (1:1), and DRT-DTX-PLGA (1 μg/mL). Results are expressed as means ± SD (n = 4). Live/dead staining assay results of different formulations on (E) U87-MG and (F) A549 cells. Calcein-AM (green) and EthD (red) was used to stain live cells, and dead cells, respectively. Scale bar: 60 μm.

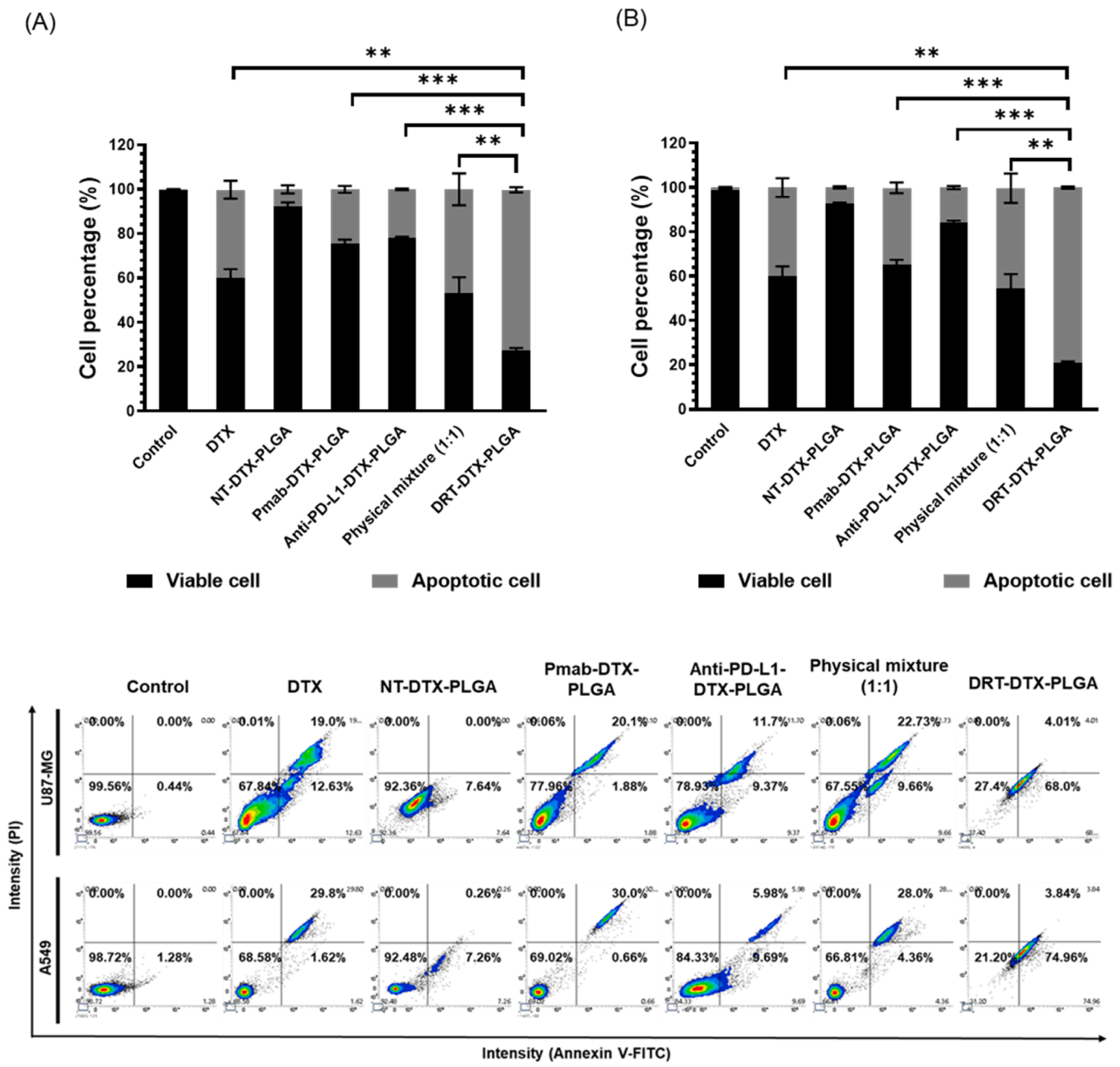

Fig. 7. *In vitro* evaluations of apoptosis. FACS analysis showed apoptosis (%) of (A) U87-MG and (B) A549 cells treated with DTX, NT-DTX-PLGA, Pmab-DTX-PLGA, anti-PD-L1-DTX-PLGA, physical mixture (1:1), and DRT-DTX-PLGA.

effect [45]. However, active targeting of these nanoparticles has led to further improvements in anti-tumor activity and therapeutic efficacy with reduced toxicity [21]. Nevertheless, the target receptor is solely overexpressed in tumor cells rather than being expressed at variable levels in healthy tissues, resulting in non-selective targeting and systematic toxicity. Moreover, due to the limited number of receptors on the target cell membrane, cellular uptake of single-ligand-modified NPs is restricted [46]. Even when the dose is increased, all biological responses reach a saturation point, and the cellular uptake is no longer increased, resulting in a saturated response [47]. To overcome non-selective targeting, the design of an effective dual-target drug delivery system enhances the cellular internalization of nanoparticles and also improves the binding affinity and avidity between the receptor and ligand [47].

In this study, EGFR and PD-L1 were selected as targeting receptors because SW480 cancer cells expressed high levels of these receptors. It has been reported that anti-EGFR and anti-PD-L1 antibodies can recognize their respective receptors and be attached to PLGA nanoparticles for effective drug delivery to target sites. Thus, we attached Pmab and anti-PD-L1 antibodies to the DTX-PLGA nanoparticles to create a single-ligand system (Pmab-DTX-PLGA and anti-PD-L1-DTX-PLGA). Furthermore, we prepared a DRT-DTX-PLGA, by attaching both Pmab and ani-PD-L1 to the surface of DTX-PLGA.

We first synthesized and analyzed Pmab-PLGA and anti-PD-L1-PLGA and then fabricated and characterized DRT-PLGA. The morphology and structure of DRT-PLGA were explored using TEM, which revealed that the gray coating was on the PLGA surface. These gray shell structures may indicate the existence of Pmab and anti-PD-L1 ligands. Surface morphology is important in determining nanoparticle uniformity and stability [48]. Pmab-PLGA, anti-PD-L1-PLGA, physical mixture (1:1), and DRT-PLGA had a larger particle size than blank PLGA, indicating the covalent linkage of antibodies on the PLGA's surface. The negative

surface charge below −20 mV suggested the presence of negatively charged carboxyl groups on the surface of the PLGA nanoparticle [49]. Furthermore, the surface charge of Pmab-PLGA, anti-PD-L1-PLGA, physical mixture (1:1), and DRT-PLGA were less negative compared to the blank PLGA that can be explained by the presence of antibodies on the PLGA nanoparticle surface. The less negative charge on the surface of Pmab-PLGA, anti-PD-L1-PLGA, physical mixture (1:1), and DRT-PLGA further improve the binding of formulation to the high negative charge cell membrane that result in increment of cellular uptake. Moreover, cationic nanoparticles are eliminated rapidly followed by anionic nanoparticle. However, slightly negative nanoparticles like Pmab-PLGA, anti-PD-L1-PLGA, physical mixture (1:1), and DRT-PLGA have the longest half-life in circulation [50]. In addition, nanoparticles with less negative charge are more stable in suspension and play a significant role in their initial adsorption of nanoparticles onto the cell membrane. After adsorption, the endocytosis uptake rate depend on the particle size and interaction of ligand with respective receptor of cell membrane [51]. Furthermore, the particle size remained unchanged for up to 24 h, verifying the stability of PLGA and other PLGA formulations. In our previous study, PLGA was found to be stable for up to 72 h [52].

The interactions between drugs and polymers were investigated using infrared spectroscopy. FT-IR analysis is a useful tool for exploring intermolecular interactions by examining shifts or broadening of spectral bands [53]. In this study, lyophilized PLGA was characterized by FT-IR and compared with blank PLGA and the pure drug. FT-IR analysis is essential for identifying chemical groups present in the drug and carrier and can provide useful information on intermolecular interactions, such as hydrogen bonds, by detecting changes in spectral peaks [54]. As shown in Fig. 2E, the spectra of the blank PLGA and DTX-PLGA were nearly identical, implying that the peaks associated with DTX were not visible. This could be attributed to the dispersion of DTX encapsulated in the molecular solution rather than the crystalline dispersion caused by the chemical interaction between the carboxylic acid of PLGA and the ester group of DTX [55–57].

The sustained-release property of nanocarriers is crucial for targeted drug delivery [58]. The more sustained DTX release behavior from DTX-PLGA can be attributed to the influence of the pH of the tumor microenvironment influencing the release properties of the nanoparticle system [59]. The slow degradation of the PLGA polymer and the strong interaction between the drug and the polymer may account for the sustained release behavior [60,61]. The initial fast release could be caused by the migration of drug molecules more quickly from the periphery and the surface of PLGA. Then slow and sustained release of drug from PLGA was observed through diffusion or time-dependent degradation of the polymeric matrix as well as progressive release of drug through the thicker drug depleted layer [62]. In acidic PBS (pH 5.5), the release of drug from PLGA was higher possibly due to the faster degradation rate of the polymer matrix at low pH, which concurs with a previous report suggesting faster degradation of PLGA under low pH conditions [19,63]. Moreover, the administration of DTX-PLGA can enhance drug pharmacokinetics in the body after drug maintenance, whether administered orally or parenterally. Furthermore, FACS and CLSM analyses of DRT-PLGA immunoreactivity assays in U87-MG and A549 cells demonstrated that the immunoreactive properties of Pmab and anti-PD-L1 were preserved after conjugation to PLGA.

Based on receptor expression analysis, we concluded that U87-MG cells express high levels of PD-L1 receptors and low levels of EGFR compared to A549 cells. Then, we evaluated the cellular uptake of DRT-C6-PLGA for dual receptor-mediated endocytosis and incubated them with U87-MG and A549 cells. The internalization of nanoparticles through non-specific binding is indicated by the spread of green fluorescence throughout the cell [64]. The single-ligand system such as Pmab-C6-PLGA and anti-PD-L1-C6-PLGA showed only a minor effect on the cellular uptake of nanoparticles, even in cells expressing EGFR and PD-L1, as shown in Fig. 5. These findings accomplished the notion that a specific ligand can facilitate nanoparticle internalization on the surface of the target cell but cannot significantly impact the cellular uptake of PLGA nanoparticles. The suppression of cellular uptake may be attributed to receptor saturation and low binding affinity, as suggested in previous studies [21,47]. Therefore, dual-targeting system was employed to enhance cell selectivity, binding affinity, therapeutic efficacy, and avidity [65,66]. The DRT system demonstrated a greater ability to bind to cells, leading to increased nanoparticle internalization compared to that of a single ligand or physical mixture [67]. In the case of a dual-targeting system with two different types of ligands, if two target receptors share the same uptake route, the specificity and affinity of the dual-targeting system for the target cells are believed to be enhanced [68]. Consequently, cellular uptake is expected to increase. Furthermore, a physical mixture of two different nanoparticles with different antibodies could increase the number of antibodies that hinder the binding of antigens to the ligands of the nanoparticles [16]. Thus, the magnitude of the uptake-mediated effect was low compared to the dual-target nanoparticles; however, it was higher than that of the single-target nanoparticles. In contrast, dual-targeted nanoparticles were designed such way that the number of each antibody was half that of the antibody number on single antibody-targeted nanoparticles. Therefore, due to the lower antibody number, steric hindrance, which limits the ligand-antigen interaction, is likely to be low for dual-targeted nanoparticles, potentially increasing the binding of nanoparticles with cells through enhanced avidity in a non-static environment [16]. According to Laginha et al., dual-targeted liposomes showed higher binding effect and uptake than that of single-targeted liposomes and showed additivity [16].

Furthermore, the limited number of receptors and endocytic recycling could hinder the effectiveness of a single ligand in enhancing nanoparticle internalization, thus restricting the number of nanoparticles available for cellular uptake [69]. However, the specific interaction between DRT-PLGA and EGFR and PD-L1 receptors enabled the nanoparticles to approach the cell surface closely and participate in electrostatic interactions, ultimately enhancing cellular uptake of DRT-PLGA [21,70].

To evaluate the cytotoxicity of DRT-DTX-PLGA in U87-MG and A549 cells, we used a CCK-8 assay. The interaction between the DRT nanoparticles and cell surface receptors determines the efficacy of DTX-loaded formulation. The CCK-8 assay showed that the sensitivities of U87-MG and A549 cells to DTX were not significantly different. Nevertheless, DRT-DTX-PLGA showed greater cytotoxic effects than DTX, NT-DTX-PLGA, Pmab-DTX-PLGA, anti-PD-L1-DTX-PLGA, and physical mixture (1:1). The cytotoxic effects of the DTX-loaded formulations were further validated using the live/dead assay (Fig. 6E and 6F) and Annexin V/PI-based apoptosis assay (Fig. 7). The data revealed that treatment with DRT-DTX-PLGA and physical mixture (1:1) led to decrease in viable cells and an increase in apoptotic cell death compared to treatment with DTX, NT-DTX-PLGA, Pmab-DTX-PLGA, and anti-PD-L1-DTX-PLGA. This can be attributed to the surface functionalization of PLGA and the intracellular accumulation of the drug concentration [71,72]. For free drug, internalization mainly occurs via molecular diffusion, and the drug concentration increases until saturation [73,74]. However, nanocarriers with and without surface modification with ligands are primarily internalized via endocytosis and then release the encapsulated drug into the cytoplasm in a sustained manner.

Furthermore, high-affinity binding to the desired target is crucial for improving detection limits and increasing therapeutic efficacy [67,75]. The receptor-antibody interaction of DRT-DTX-PLGA exhibits high binding affinity, resulting in increased intracellular DTX concentrations. This interaction enhances cytotoxicity, reduces viable cells, and increases apoptotic cells in both U87-MG and A549 cells. For example, dual-antibody-conjugated liposomes loaded with doxorubicin- were tested for the treatment of B-cell lymphoma by targeting CD20 and CD19. This liposome with dual-antibody enhanced the lifespan of mice by approximately 50% compared to doxorubicin-containing liposomes functionalizing with either anti-CD19 or anti-CD20 [76]. In another

study, Zhang et al. used dual-ligand liposomes for gene delivery for the treatment of lung cancer [77]. In their research, they used hyaluronic acid and transferrin to modify fusogenic liposomes surface that targeted lung adenocarcinoma cells, which usually express high levels of transferrin and CD44 receptors. *In vivo* study reported that the transfection efficiency of the gene was enhanced by 15% in dual-ligand liposomes-treated lung adenocarcinoma-bearing mice compared to the liposomes with single-ligand. Moreover, Liginha et al. demonstrated that dual-targeting liposomes loaded with DTX had increased cytotoxicity compared to 1:1 mixtures of liposomes targeted individually [16].

Therefore, all the data demonstrated that DRT nanoparticle showed a significant decrease in cell proliferation compared to the others, indicating the dominance of DRT-DTX-PLGA in the inhibition of cell proliferation and promotes U87-MG and A549 cell apoptosis. Hence, DRT-DTX-PLGA exhibits superior results in triggering cell death by increasing the accumulation of nanoparticle in targeted site.

5. Conclusion

In summary, Pmab and anti-PD-L1-containing ligands were synthesized and used to decorate PLGA carriers loaded with DTX. The resulting DRT-DTX-PLGA system was developed as an efficient and safe drug delivery system. *In vitro* studies showed that the dual-ligand-decorated DRT-DTX-PLGA system exhibited high cytotoxicity and enhanced drug internalization. In contrast, a single-ligand system with either Pmab or anti-PD-L1 motif was not sufficient to trigger a cytotoxic effect, whereas the dual-ligand nanosystem synergistically enhanced cellular internalization and played a key role in DTX delivery to the tumor site.

Thus, we developed a dual-ligand system to enhance the selectivity of targeted nanocarriers for better cellular uptake and cytotoxicity. This approach does not require the identification of unique ligand-receptor pairs, and its application may ultimately allow the tailoring of ligand-targeted nanocarriers to fit the profile of a particular target (tumor) system, enabling patient-specific treatments. Further experiments are necessary to determine the binding force or binding affinity between ligands of single-targeted nanoparticles and dual-targeting nanoparticles with the respective receptors of targeting cells to support the internalization of nanoparticles. Moreover, our proposed protocol anticipates future *in vivo* applications in tumor-bearing animals.

Funding

This work was supported by the Basic Science Research Program through the National Research Foundation of Korea (NRF), funded by the Ministry of Education [grant number NRF-2016R1A6A1A03011325] and by the Bisa Research Grant of Keimyung University in 2021 (Project No: 20210795) 20210795.

CRediT authorship contribution statement

Fakhrossadat Emami: Conceived the concept, Investigation, Result analysis, Writing-original draft, Writing-reviewing, and editing. **Ramesh Duwa**: Investigation, Result analysis, Writing-original draft, Writing-reviewing, and editing. **Asmita Banstola**: Investigation, Result analysis, Writing-original draft, Writing-reviewing, and editing. **Simmyung Yook**: Envisioned the concept, Investigation, Result analysis, Fund acquisition, Resources, Supervision, Writing-original draft, Writing-reviewing, and editing. **Seon Min Woo**: Result analysis, Writing-reviewing, and editing. **Taeg Kyu Kwon**: Result analysis, Writing-reviewing, and editing. All authors have read and agreed to the published version of the manuscript.

Declaration of Competing Interest

The authors declare that they have no known competing financial interests or personal relationships that could have appeared to influence the work reported in this paper.

Data Availability

Data will be made available on request.

References

[1] F.D.S.E. Melo, L. Vermeulen, E. Fessler, J.P. Medema, Cancer heterogeneity—a multifaceted view, EMBO Rep. 14 (8) (2013) 686–695.
[2] S. Urnauer, K.A. Schmohl, M. Tutter, C. Schug, N. Schwenk, S. Morys, S. Ziegler, P. Bartenstein, D.-A. Clevert, E. Wagner, Dual-targeted NIS polyplexes—a theranostic strategy toward tumors with heterogeneous receptor expression, Gene Ther. 26 (3) (2019) 93–108.
[3] N. El-Sayes, A. Vito, K. Mossman, Tumor heterogeneity: a great barrier in the age of cancer immunotherapy, Cancers 13 (4) (2021) 806.
[4] A. Marusyk, V. Almendro, K. Polyak, Intra-tumour heterogeneity: a looking glass for cancer? Nat. Rev. Cancer 12 (5) (2012) 323–334.
[5] A. Marusyk, K. Polyak, Tumor heterogeneity: causes and consequences, Biochim. Biophys. Acta - Rev. Cancer 1805 (1) (2010) 105–117.
[6] R. Baghban, L. Roshangar, R. Jahanban-Esfahlan, K. Seidi, A. Ebrahimi-Kalan, M. Jaymand, S. Kolahian, T. Javaheri, P. Zare, Tumor microenvironment complexity and therapeutic implications at a glance, Cell Commun. Signal. 18 (2020) 1–19.
[7] F. Morgillo, H.-Y. Lee, Resistance to epidermal growth factor receptor-targeted therapy, Drug Resist. Updat. 8 (5) (2005) 298–310.
[8] K. Seidi, H.A. Neubauer, R. Moriggl, R. Jahanban-Esfahlan, T. Javaheri, Tumor target amplification: implications for nano drug delivery systems, J. Control Release 275 (2018) 142–161.
[9] M. Jurczyk, K. Jelonek, M. Musiał-Kulik, A. Beberok, D. Wrześniok, J. Kasperczyk, Single-versus dual-targeted nanoparticles with folic acid and biotin for anticancer drug delivery, Pharmaceutics 13 (3) (2021) 326.
[10] Y. Zhu, J. Feijen, Z. Zhong, Dual-targeted nanomedicines for enhanced tumor treatment, Nano Today 18 (2018) 65–85.
[11] M. Bar-Zeev, Y.D. Livney, Y.G. Assaraf, Targeted nanomedicine for cancer therapeutics: towards precision medicine overcoming drug resistance, Drug Resist. Updat. 31 (2017) 15–30.
[12] J.L. Gulley, J. Schlom, M.H. Barcellos-Hoff, X.J. Wang, J. Seoane, F. Audhuy, Y. Lan, I. Dussault, A. Moustakas, Dual inhibition of TGF-β and PD-L1: a novel approach to cancer treatment, Mol. Oncol. 16 (11) (2022) 2117–2134.
[13] S. Pirkalkhoran, W.R. Grabowska, H.H. Kashkoli, R. Mirhassani, D. Guiliano, C. Dolphin, H. Khalili, Bioengineering of antibody fragments: challenges and opportunities, Bioengineering 10 (2) (2023) 122.
[14] J. Wei, Y. Yang, G. Wang, M. Liu, Current landscape and future directions of bispecific antibodies in cancer immunotherapy, Front Immunol. 13 (2022).
[15] Y. Zhou, H.L. Penny, M.A. Kroenke, B. Bautista, K. Hainline, L.S. Chea, J. Parnes, D. T. Mytych, Immunogenicity assessment of bispecific antibody-based immunotherapy in oncology, J. Immunother. Cancer 10 (4) (2022).
[16] R. Kontermann, Dual targeting strategies with bispecific antibodies. MAbs, Taylor & Francis, 2012, pp. 182–197.
[17] A. Esfandiari, S. Cassidy, R.M. Webster, Bispecific antibodies in oncology, Nat. Rev. Drug Discov. 21 (2022) 411–412.
[18] S. Mahajan, M. Aalhate, S.K. Guru, P.K. Singh, Nanomedicine as a magic bullet for combating lymphoma, J. Control. Release 347 (2022) 211–236.
[19] R. Duwa, R.H. Pokhrel, A. Banstola, M. Pandit, P. Shrestha, J.-H. Jeong, J.-H. Chang, S. Yook, T-cell engaging poly (lactic-co-glycolic acid) nanoparticles as a modular platform to induce a potent cytotoxic immunogenic response against PD-L1 overexpressing cancer, Biomaterials 291 (2022), 121911.
[20] P. Sharma, N. Kaur, A. Shanavas, Targeting strategies using PLGA nanoparticles for efficient drug delivery, poly (lactic-co-glycolic acid)(PLGA) nanoparticles for, Drug Deliv., Elsevier (2023) 123–151.
[21] G. Kibria, H. Hatakeyama, N. Ohga, K. Hida, H. Harashima, Dual-ligand modification of PEGylated liposomes shows better cell selectivity and efficient gene delivery, J. Control. Release 153 (2) (2011) 141–148.
[22] L. Mei, L. Fu, K. Shi, Q. Zhang, Y. Liu, J. Tang, H. Gao, Z. Zhang, Q. He, Increased tumor targeted delivery using a multistage liposome system functionalized with RGD, TAT and cleavable PEG, Int. J. Pharm. 468 (1–2) (2014) 26–38.
[23] M.J. Mitchell, M.M. Billingsley, R.M. Haley, M.E. Wechsler, N.A. Peppas, R. Langer, Engineering precision nanoparticles for drug delivery, Nat. Rev. Drug Discov. 20 (2) (2021) 101–124.
[24] J. Li, X. Ni, J. Zhang, Y. Liang, Z. Gao, X. Zhang, D. Zheng, D. Ding, A fluorescence and photoactivity dual-activatable prodrug with self-synergistic magnification of the anticancer effect, Mater. Chem. Front. 3 (7) (2019) 1349–1356.
[25] C. Jang, J.H. Lee, A. Sahu, G. Tae, The synergistic effect of folate and RGD dual ligand of nanographene oxide on tumor targeting and photothermal therapy in vivo, Nanoscale 7 (44) (2015) 18584–18594.
[26] Y. Mazor, A. Hansen, C. Yang, P.S. Chowdhury, J. Wang, G. Stephens, H. Wu, W. F. Dall'Acqua, Insights into the molecular basis of a bispecific antibody's target selectivity. MAbs, Taylor & Francis, 2015, pp. 461–469.
[27] J. Dong, A. Sereno, D. Aivazian, E. Langley, B.R. Miller, W.B. Snyder, E. Chan, M. Cantele, R. Morena, I.B. Joseph, A stable IgG-like bispecific antibody targeting the epidermal growth factor receptor and the type I insulin-like growth factor receptor demonstrates superior anti-tumor activity. MAbs, Taylor & Francis, 2011, pp. 273–288.

[28] Q.T. Shubhra, K. Guo, Y. Liu, M. Razzak, M.S. Manir, A.M. Alam, Dual targeting smart drug delivery system for multimodal synergistic combination cancer therapy with reduced cardiotoxicity, Acta Biomater. 131 (2021) 493–507.
[29] S. Zha, H.F. Chau, W.Y. Chau, L.S. Chan, J. Lin, K.W. Lo, W.C.S. Cho, Y.L. Yip, S. W. Tsao, P.J. Farrell, Dual-targeting peptide-guided approach for precision delivery and cancer monitoring by using a safe upconversion nanoplatform, Adv. Sci. 8 (5) (2021), 2002919.
[30] E.K. Nduom, J. Wei, N.K. Yaghi, N. Huang, L.-Y. Kong, K. Gabrusiewicz, X. Ling, S. Zhou, C. Ivan, J.Q. Chen, PD-L1 expression and prognostic impact in glioblastoma, Neuro-Oncol. 18 (2) (2015) 195–205.
[31] Z. Zhu, H. Zhang, B. Chen, X. Liu, S. Zhang, Z. Zong, M. Gao, PD-L1-mediated immunosuppression in glioblastoma is associated with the infiltration and M2-polarization of tumor-associated macrophages, Front Immunol. 11 (2020), 588552.
[32] H. Yu, T.A. Boyle, C. Zhou, D.L. Rimm, F.R. Hirsch, PD-L1 expression in lung cancer, J. Thorac. Oncol. 11 (7) (2016) 964–975.
[33] J. McLaughlin, G. Han, K.A. Schalper, D. Carvajal-Hausdorf, V. Pelekanou, J. Rehman, V. Velcheti, R. Herbst, P. LoRusso, D.L. Rimm, Quantitative assessment of the heterogeneity of PD-L1 expression in non–small-cell lung cancer, JAMA Oncol. 2 (1) (2016) 46–54.
[34] K.J. Hatanpaa, S. Burma, D. Zhao, A.A. Habib, Epidermal growth factor receptor in glioma: signal transduction, neuropathology, imaging, and radioresistance, Neoplasia 12 (9) (2010) 675–684.
[35] P.C. Burger, D.K. Pearl, K. Aldape, A.J. Yates, B.W. Scheithauer, S.M. Passe, R. B. Jenkins, C.D. James, Small cell architecture—a histological equivalent of EGFR amplification in glioblastoma multiforme? J. Neuropathol. Exp. Neurol. 60 (11) (2001) 1099–1104.
[36] D. Veale, T. Ashcroft, C. Marsh, G. Gibson, A. Harris, Epidermal growth factor receptors in non-small cell lung cancer, Br. J. Cancer 55 (5) (1987) 513–516.
[37] M.N. Koopaei, M.R. Khoshayand, S.H. Mostafavi, M. Amini, M.R. Khorramizadeh, M.J. Tehrani, F. Atyabi, R. Dinarvand, Docetaxel loaded PEG-PLGA nanoparticles: optimized drug loading, in-vitro cytotoxicity and in-vivo antitumor effect, Iran. J. Pharm. Res. 13 (3) (2014) 819.
[38] P. Kocbek, N. Obermajer, M. Cegnar, J. Kos, J. Kristl, Targeting cancer cells using PLGA nanoparticles surface modified with monoclonal antibody, J. Control. Release 120 (1–2) (2007) 18–26.
[39] W. Tao, X. Zeng, T. Liu, Z. Wang, Q. Xiong, C. Ouyang, L. Huang, L. Mei, Docetaxel-loaded nanoparticles based on star-shaped mannitol-core PLGA-TPGS diblock copolymer for breast cancer therapy, Acta Biomater. 9 (11) (2013) 8910–8920.
[40] M.R. Siddiqui, R. Railkar, T. Sanford, D.R. Crooks, M.A. Eckhaus, D. Haines, P. L. Choyke, H. Kobayashi, P.K. Agarwal, Targeting epidermal growth factor receptor (EGFR) and human epidermal growth factor receptor 2 (HER2) expressing bladder cancer using combination photoimmunotherapy (PIT), Sci. Rep. 9 (1) (2019) 2084.
[41] Z. Li, H. Huang, S. Tang, Y. Li, X.-F. Yu, H. Wang, P. Li, Z. Sun, H. Zhang, C. Liu, Small gold nanorods laden macrophages for enhanced tumor coverage in photothermal therapy, Biomaterials 74 (2016) 144–154.
[42] N. Katila, R. Duwa, S. Bhurtel, S. Khanal, S. Maharjan, J.-H. Jeong, S. Lee, D.-Y. Choi, S. Yook, Enhancement of blood–brain barrier penetration and the neuroprotective effect of resveratrol, J. Control Release 346 (2022) 1–19.
[43] A. Li, L. Zuo, Construction of anti-EpCAM drug-loaded immunomagnetic balls and its application in diagnosis of breast cancer, Nano Life 9 (01n02) (2019), 1940006.
[44] H. Kulhari, D. Pooja, S. Shrivastava, S.R. Telukutala, A.K. Barui, C.R. Patra, G.M. N. Vegi, D.J. Adams, R. Sistla, Cyclic-RGDfK peptide conjugated succinoyl-TPGS nanomicelles for targeted delivery of docetaxel to integrin receptor over-expressing angiogenic tumours, Nanomed.: Nanotechnol. Biol. Med. 11 (6) (2015) 1511–1520.
[45] T.M. Allen, P.R. Cullis, Drug delivery systems: entering the mainstream, Science 303 (5665) (2004) 1818–1822.
[46] A. Speciale, C. Muscarà, M.S. Molonia, M. Cristani, F. Cimino, A. Saija, Recent advances in glycyrrhetinic acid-functionalized biomaterials for liver cancer-targeting therapy, Molecules 27 (6) (2022) 1775.
[47] Q.C. Zheng, S. Jiang, Y.Z. Wu, D. Shang, Y. Zhang, S.B. Hu, X. Cheng, C. Zhang, P. Sun, Y. Gao, Dual-targeting nanoparticle-mediated gene therapy strategy for hepatocellular carcinoma by delivering small interfering RNA, Front. Bioeng. Biotechnol. 8 (2020) 512.
[48] H.A. Hazzah, R.M. Farid, M.M. Nasra, M.A. El-Massik, O.Y. Abdallah, Lyophilized sponges loaded with curcumin solid lipid nanoparticles for buccal delivery: Development and characterization, Int. J. Pharm. 492 (1–2) (2015) 248–257.
[49] A. Vasconcelos, E. Vega, Y. Pérez, M.J. Gómara, M.L. García, I. Haro, Conjugation of cell-penetrating peptides with poly (lactic-co-glycolic acid)-polyethylene glycol nanoparticles improves ocular drug delivery, Int. J. Nanomed. 10 (2015) 609.
[50] L. Kou, Y.D. Bhutia, Q. Yao, Z. He, J. Sun, V. Ganapathy, Transporter-guided delivery of nanoparticles to improve drug permeation across cellular barriers and drug exposure to selective cell types, Front. Pharmacol. 9 (2018) 27.
[51] M.K. Rasmussen, J.N. Pedersen, R. Marie, Size and surface charge characterization of nanoparticles with a salt gradient, Nat. Commun. 11 (1) (2020) 2337.
[52] R. Duwa, A. Banstola, F. Emami, J.-H. Jeong, S. Lee, S. Yook, Cetuximab conjugated temozolomide-loaded poly (lactic-co-glycolic acid) nanoparticles for targeted nanomedicine in EGFR overexpressing cancer cells, J. Drug Deliv. Sci. Technol. 60 (2020), 101928.
[53] J.O. Eloy, J.M. Marchetti, Solid dispersions containing ursolic acid in Poloxamer 407 and PEG 6000: a comparative study of fusion and solvent methods, Powder Technol. 253 (2014) 98–106.
[54] J.O. Eloy, R. Petrilli, J.F. Topan, H.M.R. Antonio, J.P.A. Barcellos, D.L. Chesca, L. N. Serafini, D.G. Tiezzi, R.J. Lee, J.M. Marchetti, Co-loaded paclitaxel/rapamycin liposomes: development, characterization and in vitro and in vivo evaluation for breast cancer therapy, Colloids Surf. B 141 (2016) 74–82.
[55] T. Musumeci, C. Ventura, I. Giannone, B. Ruozi, L. Montenegro, R. Pignatello, G. Puglisi, PLA/PLGA nanoparticles for sustained release of docetaxel, Int. J. Pharm. 325 (1–2) (2006) 172–179.
[56] J. Coates, Interpretation of infrared spectra, a practical approach. Encyclopedia of Analytical Chemistry, John Wiley & Sons, Ltd, US, 2000.
[57] C.-G. Keum, Y.-W. Noh, J.-S. Baek, J.-H. Lim, C.-J. Hwang, Y.-G. Na, S.-C. Shin, C.-W. Cho, Practical preparation procedures for docetaxel-loaded nanoparticles using polylactic acid-co-glycolic acid, Int. J. Nanomed. (2011) 2225–2234.
[58] R.-F. Song, X.-J. Li, X.-L. Cheng, A.-R. Fu, Y.-H. Wang, Y.-J. Feng, Y. Xiong, Paclitaxel-loaded trimethyl chitosan-based polymeric nanoparticle for the effective treatment of gastroenteric tumors, Oncol. Rep. 32 (4) (2014) 1481–1488.
[59] H. Zhang, R.-y Li, X. Lu, Z.-z Mou, G.-m Lin, Docetaxel-loaded liposomes: preparation, pH sensitivity, pharmacokinetics, and tissue distribution, J. Zhejiang Univ. Sci. B 13 (2012) 981–989.
[60] P. Rafiei, A. Haddadi, Docetaxel-loaded PLGA and PLGA-PEG nanoparticles for intravenous application: pharmacokinetics and biodistribution profile, Int. J. Nanomed. 12 (2017) 935.
[61] O.S. Qureshi, H.-S. Kim, A. Zeb, J.-S. Choi, H.-S. Kim, J.-E. Kwon, M.-S. Kim, J.-H. Kang, C. Ryou, J.-S. Park, Sustained release docetaxel-incorporated lipid nanoparticles with improved pharmacokinetics for oral and parenteral administration, J. Microencapsul. 34 (3) (2017) 250–261.
[62] F. Esmaeili, F. Atyabi, R. Dinarvand, Preparation and characterization of estradiol-loaded PLGA nanoparticles using homogenization-solvent diffusion method, DARU J. Pharm. Sci. 16 (4) (2015) 196–202.
[63] R.K. Thapa, J.Y. Choi, B.K. Poudel, T.T. Hiep, S. Pathak, B. Gupta, H.-G. Choi, C. S. Yong, J.O. Kim, Multilayer-coated liquid crystalline nanoparticles for effective sorafenib delivery to hepatocellular carcinoma, ACS Appl. Mater. Interfaces 7 (36) (2015) 20360–20368.
[64] S. Jain, G. Spandana, A.K. Agrawal, V. Kushwah, K. Thanki, Enhanced antitumor efficacy and reduced toxicity of docetaxel loaded estradiol functionalized stealth polymeric nanoparticles, Mol. Pharm. 12 (11) (2015) 3871–3884.
[65] J.M. Saul, A.V. Annapragada, R.V. Bellamkonda, A dual-ligand approach for enhancing targeting selectivity of therapeutic nanocarriers, J. Control. Release 114 (3) (2006) 277–287.
[66] Y. Murase, T. Asai, Y. Katanasaka, T. Sugiyama, K. Shimizu, N. Maeda, N. Oku, A novel DDS strategy,"dual-targeting", and its application for antineovascular therapy, Cancer Lett. 287 (2) (2010) 165–171.
[67] J.F. Stefanick, D.T. Omstead, T. Kiziltepe, B. Bilgicer, Dual-receptor targeted strategy in nanoparticle design achieves tumor cell selectivity through cooperativity, Nanoscale 11 (10) (2019) 4414–4427.
[68] K. Takara, H. Hatakeyama, N. Ohga, K. Hida, H. Harashima, Design of a dual-ligand system using a specific ligand and cell penetrating peptide, resulting in a synergistic effect on selectivity and cellular uptake, Int. J. Pharm. 396 (1–2) (2010) 143–148.
[69] Z. Yang, W. Tang, X. Luo, X. Zhang, C. Zhang, H. Li, D. Gao, H. Luo, Q. Jiang, J. Liu, Dual-ligand modified polymer-lipid hybrid nanoparticles for docetaxel targeting delivery to Her2/neu overexpressed human breast cancer cells, J. Biomed. Nanotechnol. 11 (8) (2015) 1401–1417.
[70] K. Takara, H. Hatakeyama, G. Kibria, N. Ohga, K. Hida, H. Harashima, Size-controlled, dual-ligand modified liposomes that target the tumor vasculature show promise for use in drug-resistant cancer therapy, J. Control Release 162 (1) (2012) 225–232.
[71] F. Emami, A. Banstola, A. Vatanara, S. Lee, J.O. Kim, J.-H. Jeong, S. Yook, Doxorubicin and anti-PD-L1 antibody conjugated gold nanoparticles for colorectal cancer photochemotherapy, Mol. Pharm. 16 (3) (2019) 1184–1199.
[72] Z. Gu, Q. Wang, Y. Shi, Y. Huang, J. Zhang, X. Zhang, G. Lin, Nanotechnology-mediated immunochemotherapy combined with docetaxel and PD-L1 antibody increase therapeutic effects and decrease systemic toxicity, J. Control. Release 286 (2018) 369–380.
[73] C. Shi, Z. Zhang, J. Shi, F. Wang, Y. Luan, Co-delivery of docetaxel and chloroquine via PEO–PPO–PCL/TPGS micelles for overcoming multidrug resistance, Int. J. Pharm. 495 (2) (2015) 932–939.
[74] C.H. Kim, T.H. Kang, B.D. Kim, T.H. Lee, H.Y. Yoon, Y.T. Goo, Y.S. Choi, M.J. Kang, Y.W. Choi, Enhanced docetaxel delivery using sterically stabilized RIPL peptide-conjugated nanostructured lipid carriers: In vitro and in vivo antitumor efficacy against SKOV3 ovarian cancer cells, Int. J. Pharm. 583 (2020), 119393.
[75] K.D. Orcutt, J.J. Rhoden, B. Ruiz-Yi, J.V. Frangioni, K.D. Wittrup, Effect of small-molecule–binding affinity on tumor uptake in vivo: a systematic study using a pretargeted bispecific antibodyaffinity and tumor uptake, Mol. Cancer Ther. 11 (6) (2012) 1365–1372.
[76] P. Sapra, T.M. Allen, Improved outcome when B-cell lymphoma is treated with combinations of immunoliposomal anticancer drugs targeted to both the CD19 and CD20 epitopes, Clin. Cancer Res. 10 (7) (2004) 2530–2537.
[77] B. Zhang, Y. Zhang, D. Yu, Lung cancer gene therapy: transferrin and hyaluronic acid dual ligand-decorated novel lipid carriers for targeted gene delivery, Oncol. Rep. 37 (2) (2017) 937–944.